REPUBLIC OF TURKEY
ADANA ALPARSLAN TÜRKEŞ SCIENCE AND TECHNOLOGY UNIVERSITY

GRADUATE SCHOOL OF NATURAL AND APPLIED SCIENCES
DEPARTMENT OF BIOENGINEERING

THEORETICAL MODELING OF HETEROLYTIC MECHANISM FOR H_2 PRODUCTION: A DETAILED INVESTIGATION OF COBALT(II)-POLYPYRIDYL CATALYST

AYAS KİSER

MASTER OF SCIENCE

ADANA YEAR

REPUBLIC OF TURKEY
ADANA ALPARSLAN TÜRKEŞ SCIENCE AND TECHNOLOGY UNIVERSITY

GRADUATE SCHOOL OF NATURAL AND APPLIED SCIENCES
DEPARTMENT OF BIOENGINEERING

THEORETICAL MODELING OF HETEROLYTIC MECHANISM FOR H_2 PRODUCTION: A DETAILED INVESTIGATION OF COBALT(II)-POLYPYRIDYL CATALYST

AYAS KİSER
MASTER OF SCIENCE

SUPERVISOR
ASSOC. PROF. YELİZ GÜRDAL DURĞUN

ADANA 2022

Theoretical Modeling of Heterolytic Mechanism for H_2 Production: A Detailed Investigation of Cobalt(II)-Polypyridyl Catalyst

submitted by **Ayas KİSER** in partial fulfillment of the requirements for the degree of **Master of Science in Department of Bioengineering, Adana Alparslan Türkeş Science and Technology University** by,

Assoc. Prof. Dr. Ahmet BEYCİOĞLU
Graduate School Director

Prof. Dr. Gözde BAYDEMİR PEŞİNT
Department Chair

Assoc. Prof. Dr. Yeliz GÜRDAL DURĞUN
Supervisor

Thesis Committee

Supervisor
Assoc. Prof. Dr. Yeliz GÜRDAL DURĞUN

Adana Alparslan Türkeş Science and Technology University

Asst. Prof. Dr. Tolga KARAZEHİR
Adana Alparslan Türkeş Science and Technology University

Asst. Prof. Dr. Onur DÖKER
Mersin University

Thesis Defense Date

28/07/2022

I hereby declare that all information in this thesis has been obtained and presented in accordance with academic rules and ethical conduct. I also declare that, as required by these rules and conduct, I have fully cited and referenced all information that is not original to this work.

[Signature]

Ayas KİSER

ABSTRACT

Theoretical Modeling of Heterolytic Mechanism for H_2 Production: A Detailed Investigation of Cobalt(II)-Polypyridyl Catalyst

Ayas KİSER

Department of Bioengineering

Supervisor: Assoc. Prof. Yeliz Gürdal Durğun

July 2022, 60 pages

Hydrogen (H_2) molecule is a remarkable carrier of energy that is found naturally in biomass, water, and hydrocarbon. Solar energy is the most abundant energy source, which plants inherently uses to feed their photosynthesis mechanisms. Hereupon, researchers gain inspiration of these nature's great event, the light reactions of impeccable H_2 production pathway of photosynthesis. In order to mimick the water reduction mechanism of photosynthesis, various transition metals have been employed. However, a satisfactory solution couldn't been found in the terms of price/performance ratio. Recently, researchers have investigated photocatalytic water reduction by taking advantage of Cobalt based photocatalysts. In this connection, by applying Ab-initio Molecular Dynamics simulations as well as Density Functional Theory, and Free Energy Perturbation Theory, we investigate water reduction, also known as H_2 production, mechanism of Co-based poly-pyridyl catalyst having perfect octahedral coordination. At this thesis, our aim is to clarify the effect of regulation at octahedral coordination and compare the two pathways of, ECEC and EECC, H_2 production mechanism. Consequently, for the hydrogen production cycle, both ECEC and EECC mechanisms are utilized and each intermediate step is simulated in order to determine the allowed spin states as well as solvent response around the reaction center of Co-based water reduction catalyst investigated. Furthermore, by performing additional simulations the electronic structures of each intermediate step of both mechanisms have been analyzed. Reduction free energies have been calculated using Marcus theory of electron transfer.

Keywords: Ab-initio molecular dynamics, Density Functional Theory, water reduction, reduction free energy

ÖZET

H_2 Üretimi Heterolitik Mekanizmasının Teorik Modellemesi: Kobalt(II)-Polipiridil Katalizörünün Detaylı Olarak İncelenmesi

Ayas Kiser
Biyomühendislik Anabilim Dalı
Danışman: Doç. Dr. Yeliz Gürdal Durğun
Temmuz 2022, 60 sayfa

Hidrojen (H_2) molekülü biyokütle, su ve biyokarbonun içerisinde doğal olarak bulunan bir enerji taşıyıcısıdır. Güneş enerjisi ise bitkilerin fotosentez mekanizmalarında doğal olarak kullandıkları en yaygın bulunan enerji kaynağıdır. Araştırmacılar doğanın önemli bir olayı olan fotosentezin ışıklı reaksiyonlarındaki kusursuz H_2 üretme yolağından ilham almışlardır. Fotosentezin su indirgeme mekanizmasını taklit etmek amacıyla çok çeşitli geçiş metalleri kullanılmıştır. Buna rağmen araştırmacılar, kobalt bazlı fotokatalizörleri keşfedene kadar, fiyat/performans açısından tatmin edici bir cevap bulamamışlardır. Yakın zamanda, Kobalt bazlı fotokatalizörler kullanılarak fotokatalitik su indirgemesi üzerine bir çok araştırma yapılmıştır. Bu bağlamda, tezimizde düzgün dörtyüzlü koordinasyona ve çoklu piridil grubuna sahip Co-bazlı katalizörün su indirgeme, bir diğer adıyla, H_2 üretme mekanızması Ab-initio moleküler dinamik, Yoğunluk Fonksiyoneli Teorisi ve Serbest Enerji Pertürbasyon Teorisi kullanılarak incelenmiştir. Bu tezdeki amacımız, oktahedral koordinasyondaki düzenlemenin etkisini açıklığa kavuşturmak ve ayrıca, heterolitik H_2 üretme mekanizmasının yolaklarından ikisi olan ECEC ve EECC mekanizmalarını karşılaştırmaktır. Dolayısıyla, çalışma boyunca, hidrojen üretim döngüsünün ECEC ve EECC mekanizmaları değerlendirilerek, mekanizmanın her ara adımı simüle edilmiş ve ayrıca Co-bazlı su indirgeme katalizörünün çevresindeki çözelti tepkisi incelenmiştir. Buna ek olarak, her iki mekanizmanın her bir adımının elektronik yapıları ek simülasyonlar uygulanarak analiz edilmiştir. Elektron transferi için Marcus Teorisi kullanılmış ve indirgenme serbest enerjileri hesaplanmıştır.

Anahtar Kelimeler: Ab-initio moleküler dinamik, Yoğunluk Fonksiyoneli Teorisi, su indirgeme, indirgenme serbest enerjisi

dedication

to my future children

please understand how difficult conditions I have survived to feed you.

ACKNOWLEDGEMENTS

I think it would be best to begin my appreciation with this meaningful and valuable quote:
“A word you say to someone, a favor you did, doesn't fade away. If you make someone laugh, for example, it doesn't fly away, it leaves a mark on cheek, maybe a thousand years…”
I would like to convey my respects and thanks to my supervisor *Assoc. Prof. Yeliz Gürdal Durğun* for her great support to my education with her knowledge and experience. Above all, I would like to express my gratitude to her for giving me a place in this project, for holding my hand in giving direction to my life, which I could not achieve on my own. I would like to thank my friends from my research group, *İpek Güçlü*, for not only being my project partner for two years, but also for quietly supporting me during my hard times and laughing even at my bad jokes so as not to offend me and *Tuğçe Gökdemir* for making jokes at least as bad as I did and for being able to laugh even at them together as well as her beautiful energy. I appreciate my dearest friends *Ceren Deran* and *Damla Tireng* who trust me even more than I do during these two years. I would like to thank them for not leaving me alone and showing up when I needed support, and for patiently listening to even the topics I just learned that were boring to them but that I couldn't stop talking about. I would like to thank to my dear family whose existence I am always grateful for, to my dear father *Ayhan Kiser*, who taught me that I have to fight under all circumstances, to my dear mother *Aslı Kiser*, who I took my strength from, and to my siblings *Çağla* and *İbrahim Halil Kiser*, who always supported me whenever and wherever they were, and last but not least, my dear brother *Umut Toklar*, who was always my emotional support and still is.

One last word, thank you *all* for the mark on my cheek which I believe it will remain until the end.

I would like to acknowledge the Scientific and Technological Research Council of Turkey (TUBITAK). This study has received funding from the TUBITAK under the 3501 Career Development Program (grant agreement No: 120Z240). The calculations reported in this thesis have been performed at the TUBITAK ULAKBIM, High Performance and Grid Computing Center (TRUBA), based in Turkiye.

TABLE OF CONTENTS

LIST OF FIGURES

LIST OF TABLES

NOMENCLATURE

PSI	: Photosystem I
PSII	: Photosystem II
HEP	: Hydrogen Evolution Photocatalyst
OEP	: Oxygen Evolution Photocatalyst
CO_2	: Carbondioxide
ATP	: Adenosine triphosphate
DC	: Direct current
H_2O	: Water molecule
Pt	: Platinum
h+	: Proton
e-	: Electron
Co	: Cobalt
Ru	: Ruthenium
C	: Carbon
H	: Hydrogen
N	: Nitrogen
O	: Oxygen
Ar	: Argon
ps	: picosecond
Å	: Angstrom
K	: Kelvin
eV	: Electron Volt
TON	: Turnover Number
DFT	: Density Functional Theory
pH	: Potential of Hydrogen
V	: Volt
MD	: Molecular Dynamics
TOF	: Turnover Frequency
SHE	: Standard Hydrogen Electrode

AIMD	: Ab-Initio Molecular Dynamics
ρ	: Density
HOMO	: Highest Occupied Molecular Orbital
LUMO	: Lowest Unoccupied Molecular Orbital

1 INTRODUCTION

Demand of energy need associated with population increase, has obliged authorities to redress this requirement and deflect away from fossil energy sources (Lewis & Nocera, 2006). Our world faces with a supreme challenge for a long while, causing climate change, goes by the name of greenhouse warming. Although the primary concern is to focusing on environmental issues, climate change feature in impairment of human health in parallel with causing to poor quality of food and air (Watts et al., 2021). Circumstantially, in the light of environmental health, overcoming this major energy problem by replacing fossil fuels with clean and sustainable energy sources is crucial (Lewis & Nocera, 2006). In this connection, solar energy attracts the attention due to secure energy, accesibility and infinite source features (Lewis & Nocera, 2006; Teets & Nocera, 2011). In the matter of using solar energy, the first thing come to mind is natural photosynthesis of green plants. Photosynthesis is an important process whereby it is been looked with admiration ever since it descried. At this system, a double excitation process is supplied by the use of two protein structures within thylakoid membrane of chloropyhll, named photosystem I (PSI) and photosytem II (PSII). Reduction and oxidation changes of light reactions at photosynthesis, associated with excitation of electrons appertain to PSI and PSII, through photons from sunlight, termed as Z-scheme, see Figure 1. Several studies have been performed in order to illuminate the double excitation process of natural photosynthesis as well as it have been practised inspired by natural photosynthesis and mimicking the Z-scheme process by utilising two narrow band semiconductors as hydrogen evolution photo-catalyst (HEP) and oxygen evolution photo-catalyst (OEP) is achieved (Y. Wang et al., 2018).

Researchers interested in the topic, amazed by the concept of capturing solar energy and convert it into fuels since Edmond Becquerel, the french scientist first study out the photoelectric effect (Grätzel, 2010). In consequence, amongst diverse recipes of transforming solar energy into practicable conformation, the most preferred is Hydrogen (H_2) as a clean energy carrier (Kong et al., 2018). Hydrogen production technology through solar energy, take notice of authorities in this context, by means of clean energy source and long dated

answer of lowering atmospheric CO_2 levels (Dresselhaus et al., 2004; Esswein & Nocera, 2007).

Underlying technique of achieving H_2 production through solar radiation has been discovered long ago by taking inspiration from nature. Fundamentally, for providing energy to their system, plants has been using phosphate bonds within ATP, concordantly using H bonds within H_2 can be applicable via recovering water molecules (Esswein & Nocera, 2007). Within this concept, several versions of capturing solar energy in order to produce hydrogen, such as electrolysis, photocatalytic water splitting, hydrolysis has been studied (Anantharaj et al., 2018). In between, electrolysis of water is the most commonly used one based on a system which includes an anode, cathode, electrolyde and power source. A direct current applied from negative terminal of the power supply to the cathode enables H_2 generation at the cathode through reduction of protons. On the other part, O_2 production take place along with oxidation of hydroxyl groups and at the same time, electrons which produced via electrochemical reaction returns to the positive terminal of the power supply.

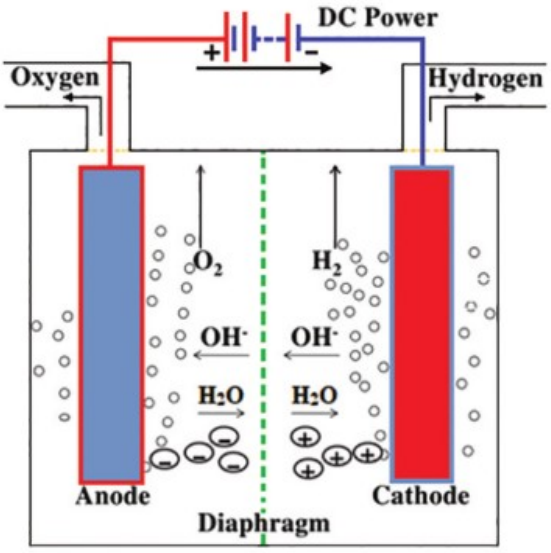

Figure 1: A representation of electrolysis system in water. Anode and cathode sides are separated by a diaphragm. Hydrogen gas from cathode compartment and Oxygen gas from anode compartment be constituted (Naimi & Antar, 2018).

The catalytic splitting of water into H_2 and O_2 in electrolysis requires an extrinsic energy supply. It is shown that, this energy supply can be reduced by the use of high acidic solutions (Rossmeisl et al., 2007). In order to enhance H_2 production rate, acidic conditions are required (Anantharaj et al., 2016). Pt included catalysts have the best performance under acidic conditions on the purpose of H_2 production. The catalysts which based on Pt, Ir and Ru reduce the over-potential for water electrolysis, however, the expenses and percentage of availability in nature of these transition metals slog on to promote large scale production (Anantharaj et al., 2018). Through the agency of photocatalytic water reduction mechanism, H_2 energy can be also acquired from solar energy (Kong et al., 2018). Break down water into H_2 and O_2 through photo-catalytic water splitting is an alternative and conspicuous method, by virtue of redefine H_2 energy as an entire renewable energy source, thereby benefit from solar energy instead of electrical energy (Grätzel, 2010).

In order to produce molecular hydrogen, employing photo-catalytic water splitting mechanism can put into practice by means of heterogeneous and homogeneous systems. Since the water splitting mechanism investigated by researchers, focus of interest was heterogeneous systems, thus, homogeneous systems remain in the background for a long time. Contrary to this, during the recent years the studies have been revolved around to comprehend the homogeneous systems and improving these systems are in high demand. Following the studies and searches regarding heterogeneous and homogeneous systems, it is been revealed that both systems are in accordance with water reduction mechanisms, however at the same time, both have their downsides and challenges (M. Wang et al., 2009). Compared to the heterogeneous catalysts, homogeneous catalysts combined with transition metal complexes for solar-driven hydrogen generation methods have been studied a lot fewer until 2000. Accordingly, in order to achieve large scale production of H_2 along with solar radiation, usage of low costs homogeneous catalysts has draw attention in recent years (M. Wang et al., 2009).

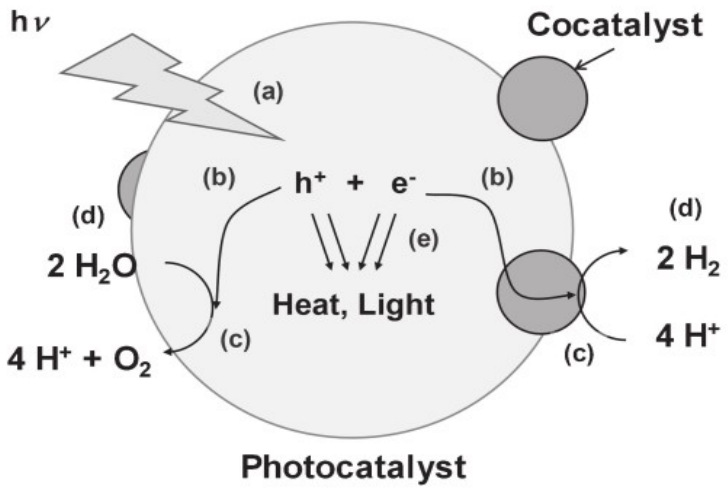

Figure 2: Main steps of photocatalytic water splitting process on a heterogeneous photocatalyst. (a) Light absorption, (b) charge transfer, (c) redox reactions, (d) adsorption, desorption, and mass diffusion of different kind of chemical structures, and (e) charge-hole recombination (Hisatomi et al., 2012) .

As the main principle of the heterogeneous system, photosensitiser at the reaction medium excites by a photon and then transfers the electron to the water reduction catalyst. Electrons and the protons of water molecule generates H_2 molecule at the reaction center of the photocatalyst. In the meantime the oxidated photosensitiser then receives electron from electron donor at the medium and returns to the ground state as depicted in Figure 2. Associated with use of homogeneous catalysts, water splitting processes can be fully employed with the benefit of having tunable systems. However, it is in fact easier and applicable to implement these two processes separately (Guttentag et al., 2012). The studies in literature mostly depends on exclusively water reduction or water oxidation, on the occasion of photocatalytically complication of the system increases at the same reaction medium where both reduction and oxidation occurs. In order to prevent this complexity, over the course of photocatalytic H_2 production, instead of using catalyst for water oxidation, sacrificial electron donors were used and it is showed that it is oxidated without effecting the water reduction reaction mechanism (Probst et al., 2010). Even though the value of homogeneous catalysts have been appreciated posteriorly, water reduction systems using homogeneous catalysts have been investigated and found to be world shacking in terms of having substantial characteristics for practical application such as long term stability and increased efficiency due to the covalent bond between catalyst and photosensitizer (M. Wang et al., 2009).

It is been a contemporary topic to investigate H_2 production mechanism of transition metal based molecular catalysts in aqueous reaction environment (M. Wang et al., 2009). Within these enquiries, even though they increase reaction activation, it is economically not advantageous to use expensive transition metals like Platin (Pt) for large scale production (Esswein & Nocera, 2007). Instead of precious metals, e.g. Pt, Ru, in this project less expensive metal Cobalt (Co) based catalysts will be investigated.

H_2 production mechanism of Co-based polypyridyl ligands through photochemical reduction mechanism have not been entirely understood by the reason of limited availability of experimental and theoretical studies in literature (Queyriaux et al., 2015). Several catalysts can be synthesized having different properties like design, pyridyl number and location around transition metal and structural symmetry (Joliat et al., 2016; Probst et al., 2011). In the literature many different ligand types tuneful with Co-based catalysts have been investigated such as porphyrin (C. H. Lee et al., 2011), cobaloxime (Bhattacharjee et al., 2013) and polypyridine ligands (Gurdal & Iannuzzi, 2020; Guttentag et al., 2012). Among them, by virtue of having high stability and strong ligand field as well as showing higher catalytic activities, polypyridyl ligands lead the role (Leung et al., 2012; Sun et al., 2011). It is revealed that catalytic activity of the system can be affected by number, symmetry and configurations of pyridyl groups around Co center (Queyriaux et al., 2015). A range of results from performed experiments have shown that the ligand structure of the catalysts affects catalytic activity. It is introduced that ligand coordinations of polypyridyl groups have profound impact on H_2 production rate (Bachmann et al., 2013).

The cobalt based penta-pyridyl ligands, CoPPy, which consists of two hydroxy functions and five pyridine units have been investigated, synthesized and experimental studies carried out to ascertain water reduction performance by Prof. Roger Alberto and his study group in Chemistry Department of University of Zurich. The results of experimental studies have shown that cobalt based penta-pyridyl ligands, CoPPy lead to high H_2 turnover numbers. This study demonstrates that the configurations of penta-pyridyl ligands around Co center have a voice in the catalytic activity of the system (Bachmann et al., 2013). In more recent times, following the study of Bachmann et al., a theoretical study published by (Gurdal & Iannuzzi, 2020) in the matter of comparing distorted octahedral arrangement structured Co based penta and tetra pyridyl ligands. In this study, they carried out a series of theoretical and computational studies, in order to enlighten their mechanisms, compare their performances

and reveal their distinctive characteristics (Gurdal & Iannuzzi, 2020). However, perfect octahedral coordination structured penta and tetra pyridyl ligands not yet enlightened and accordingly, the studies on comparison and effects of distorted and perfect octahedral structured ligand types are still deficient. Investigation of perfectly oriented penta-pyridyl ligand type is important also due to discuss the electronic details of the system by comparing the structural effects with distorted orientation of Co based penta-pyridyl ligands hard-labored at the recent study of (Gurdal & Iannuzzi, 2020). At the given study, strongly distorted structured Co based penta and tetra pyridyl ligands have been examined in detail, including literature research and theoretical simulations. Therebeside, same as the constitutionally distorted penta-pyridyl ligands, there are limited studies about perfectly oriented Co based penta-pyridyl ligands which comprehensively represented involving all the steps of the water reduction reaction (Gürdal, 2017). In this regard, this thesis focused on investigating homogeneous Co based catalyst having perfectly oriented penta-pyridyl ligands through the instrument of Density Functional Theory based simulations.

2 LITERATURE REVIEW

The studies on mechanism of photo-chemical reduction reaction and H_2 production of Co-based poly-pyridyl ligands are limited in literature as both experimentally and theoretically (Queyriaux et al., 2015). In this part of the thesis, we summarize current state of the art for photo-chemical H_2 production using homogeneous Co based catalysts. The results of experimental and theoretical studies as well as inadequacies in the literature will be addressed.

Studies on Co-based Poly-pyridyl Catalysts Performed for Water Reduction Reaction

Among several suggested Co centered catalysts come to light that are active in homogeneous environment, in our study we focus on penta-pyridyl ligand based Co photo-catalyst abbreviated as CoPPy. Penta-pyridyl ligand structured Co-based catalyst is synthesized by Prof. Roger Alberto and his research team in Chemistry department of the University of Zurich. It consists of five pyridine rings with a backbone endowed with two hydroxy functions (Bachmann et al., 2013).

An experimental study performed by (Bachmann et al., 2013) investigates H_2 production performances of pentadentate $CoPy_5$ and $Co(bPy)_2Py$ as well as tetradentate $Co(bPy)Py_2$ catalysts, given at Figure 3-(a)-(b), using cyclic voltammogram and high performance liquid chromatography techniques. $CoPy_5$ and $Co(bPy)_2Py$ both have two bi-pyridyl and one pyridyl groups in their structures, whereas $Co(bPy)Py_2$ includes one bi-pyridyl and two pyridyl groups surrounding the Co center. While $CoPy_5$ shows perfect octahedral coordination around the Co center, $Co(bPy)_2Py$ and $Co(bPy)Py_2$ show distortions from the pentadentate coordinations. According to the results, both $Co(bPy)_2Py$ and $Co(bPy)Py_2$ show higher H_2 production rate with respect to $CoPy_5$, implying that the ligand structures around Co and distortions from the octahedral arrangement are important criterias for achieving high water reduction rates. The Co(II/I) reduction potentials of $CoPy_5$ and $Co(bPy)_2Py$ are measured as -1.3 V and -0.87 V, respectively.

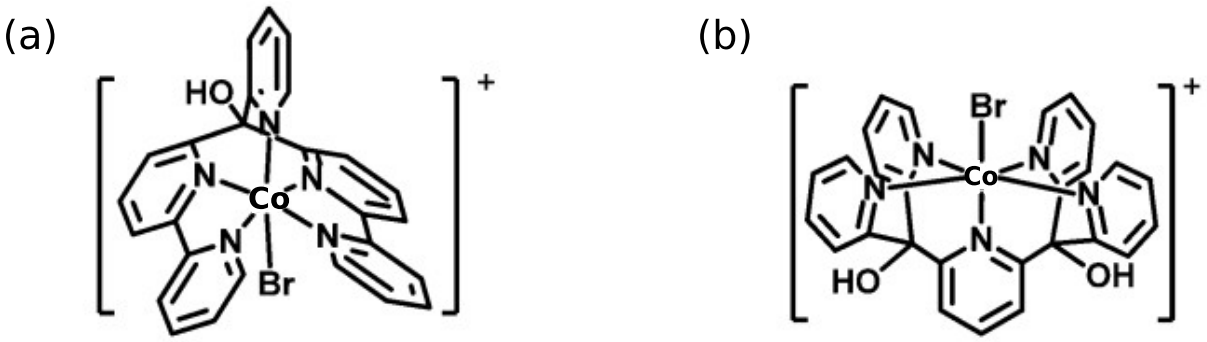

Figure 3: Schematic representations of Co based penta-pyridyl catalysts with alternative Pentapyridine ligand frameworks, (a) pentapyridine structure with almost perfect octahedral arrangement, (b) Less symmetric pentapyridine structure with two bipyridine units and one pyridyl donor (Bachmann et al., 2013)

(Queyriaux et al., 2018) have studied novel tetra-pyridyl cobalt complex, $[Co(bapbpy)(H_2O)_2]^{2+}(1^{2+})$, abbreviated as $1(BF_4)_2$ which has a distorted octahedral geometry, see Figure 4-(a). They achieved 443 TONs H_2/Co which corresponds to 3 mL of H_2 production under visible light as depicted in Figure 4-(b). Their study revealed that ECEC sequence is more likely to occur with compared to the ECCE mechanism where E stands for reduction and C stands for protonation steps of the H_2 production reaction. The sequence of reduction and protonation steps might differ for some of the catalysts which forms EECC and ECEC mechanisms. ECCE pathway is unlikely to progress for the catalyst under consideration due to the neutral reaction environment. However, the detailed catalytic mechanism of the $1(BF_4)_2$ complex has not been investigated in detail.

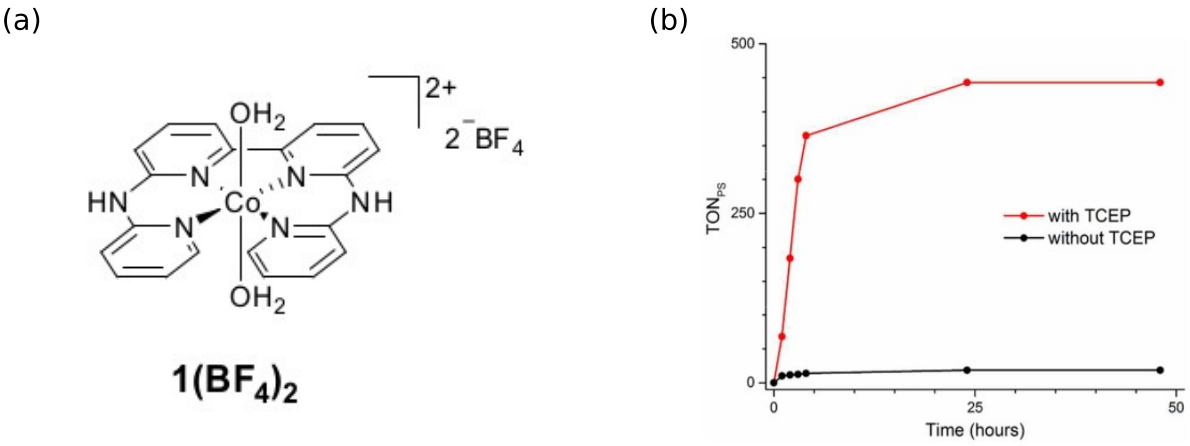

Figure 4: (a) Schematic representation of cobalt tetra-pyridyl complex $1(BF_4)_2$. (b) The H_2 production activity of $1(BF_4)_2$ in an aqueous solution at pH 4.5 under visible light-driven conditions (Queyriaux et al., 2018).

A series of experimental and theoretical studies have been carried out by (Lucarini et al., 2021) in order to reveal the effects of modification of ligands on H_2 production activities. They characterized hexadentate ligands and substitute $-CF_3$, electron-withdrawing groups (EWG), and $-OCH_3$, electron donating groups (EDG), to bipyridine and pyridine ligands of the cobalt polypyridine complexes. As a result of the study, it is revealed that the substituent kind is less effective when compared to the location of the substituents. Besides, the catalytic performance of complexes increases when a substitution, EWG or EDG, introduced to the pyridine ligand of the catalyst.

(Xie et al., 2014) experimentally investigated the comparison of photocatalytic H_2 production activities belonging to four Co based catalysts having same pentadentate arrangement but different monodentate ligands, $[Co^{III}(N4Py)Cl]^{2+}$(1), $[Co^{III}(N4Py)(NO_3)]^{2+}$ (2), $[Co^{III}(N4Py)(SO_3CF_3)]^{2+}$ (3), and $[Co^{III}(N4Py)(H_2O)]^{3+}$ (4), (N4Py = 1,1-di(pyridin-2-yl)-N,N-bis(pyridin-2-ylmethyl)methanamine), see Figure 5-(a). Experimental studies have been carried out in order to find out the role of the monodentate ligands on H_2 production rate and results show that photocatalytic activities of the catalysts highly depend on chemical nature of the monodentate ligands, see Figure 5-(b). The pyridine ligand of the N4Py dissociates from the Co center during the reaction cycle. Besides, it is revealed that Co(III) hydride formation as an intermediate step depends on the presence of the pyridine ligand. Depending on the coordination of the Co center with the pyridine group as well as pH of the solution, the dissociation from the Co center may result in two possibilities, Co(II) or Co(III).

(a)

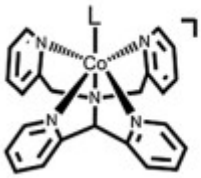

n+ L= Cl^-, n=2 **1**

NO_3^-, n=2 **2**

$CF_3SO_3^-$, n=2 **3**

H_2O, n=3 **4**

(b)

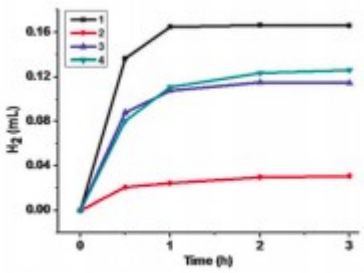

Figure 5: (a) Schematic representation of Co(III) based photocatalysts. (b) H_2 production rate of $[Co^{III}(N4Py)Cl]^{2+}$(1), $[Co^{III}(N4Py)(NO_3)]^{2+}$ (2), $[Co^{III}(N4Py)\text{-}(SO_3CF_3)]^{2+}$ (3), and $[Co^{III}(N4Py)(H_2O)]^{3+}$ (4) in water (Xie et al., 2014).

(Rodenberg et al., 2015) have investigated the H_2 production reactivity of $Co(bPy)Py_2$ applying both experimental and theoretical approaches. In this context, theoretical studies have been carried out under vacuum and it is demonstrated that following the first electron injection, the spin multiplicity of the formed intermediate state, Co(I), has two possibilities as singlet or triplet spin states. Following this, they emphasized that the production cycle proceeds with heterolytic ECEC mechanism and Co(III)-H hydride formed as a reaction intermediate. By applying DFT simulations, it is calculated that the triplet spin state of the Co(I) intermediate has lower potential energy than the its counterpart having singlet spin state. However, the reaction proceeds with the singlet spin state and the probable reason of this observation remains unexplained. Furthermore, one another heterolytic mechanism, EECC, has been eliminated in this study and the Co spin states at each intermediate steps have been determined.

Associated with electrochemical and spectroscopic studies, (Alberto et al., 2019) have investigated reduction and protonation potentials of $Co(bPy)Py_2$ for H_2 production and have provided a Pourbaix diagram which shows alteration of the mentioned potentials. Heterolytic ECEC H_2 production mechanism has been investigated, which consists consecutive electron injection and protonation steps. As a result of the AIMD simulations, two possibilities of continuation of the ECEC mechanism, both triplet and singlet spin states give similar energies From the analysis of the obtained AIMD trajectories as well as distribution of molecular orbitals, it is emerged that the first protonation reaction is likely to continue with the singlet spin state. The EECC mechanism, on the other hand, remains unsurveyed in the study.

(Schnidrig et al., 2017) have investigated H_2 production performances of several catalysts possessing different poly-pyridyl ligands in their structures depicted in Figure 6-(a), (b) and (c). For instance, in this study, it is demonstrated that $Co(bPy)_2CO$ (5) show high stability and 20 nmol H_2/s reaction rate under optimum conditions have been acquired, see Figure 6-(d). The study has revealed that reaction rate depends on amount of proton within the reaction medium and it increases with enhanced acidic conditions. On the other hand, the effects of coordination differences of the catalysts on activity has not been discussed in the study.

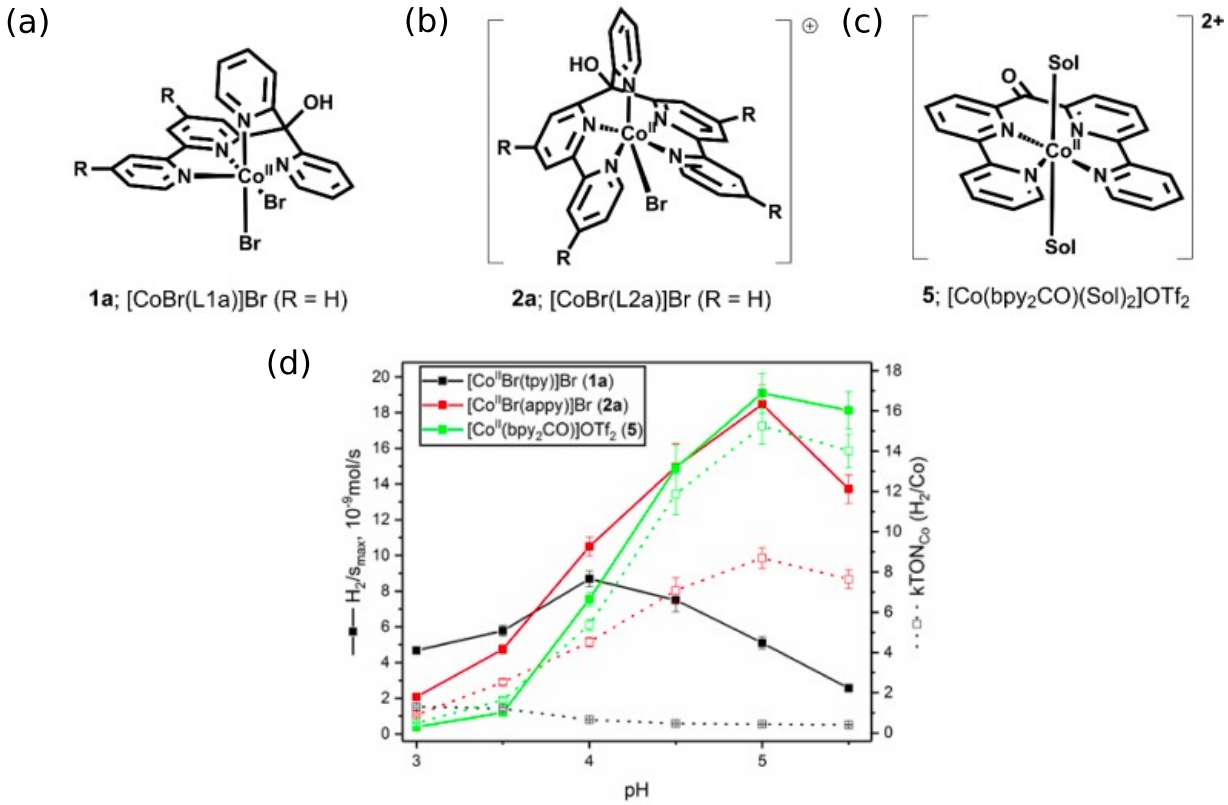

Figure 6: Schematic representations of Co based catalysts (a) $[Co^{II}Br(tpy)]Br$, (b) [CoBr(appy)]Br and (c) $[Co(bpy_2CO)(Sol)_2]OTf_2$. (d) Reaction rates of $[Co^{II}Br(tpy)]Br$, [CoBr(appy)]Br and $[Co(bpy_2CO)(Sol)_2]OTf_2$ abbreviated as 1a, 2a and 5, respectively, are given depending on pH. Dashed lines represent TON of given catalysts assigned to corresponding colors (Schnidrig et al., 2017).

Co based penta-pyridyl ligand catalysts having two methyl or trifloromethyl groups in their structures have been investigated by (Sun et al., 2011). Experiments reveal that the catalyst employed trifloromethyl groups seems to acquire more positive Co(II)/Co(I) reduction potential as -0.76 vs SHE. However, the other intermediate steps of the reaction remain unevaluated.

(Song et al., 2017) have studied photocatalytic H_2 production activity of two linear aminopyridine ligand 2,6-bis[(methyl(pyrid-2-ylmethyl)amino)-N-methyl]pyridine complexes abbreviated as $[M(Py^{Me}pam)](BF_4)_2$, M=Co (1) and M=Zn (2). At this study they synthesized the complexes, see Figure 7-(a), and then compare their water reduction activity by employing electrochemical studies. As a result of the experiments, from Co based complex under optimized conditions highest TON of 290 has been achieved for H_2 production, see Figure 7-(b). Contrary to this, (2) has shown low catalytic activity.

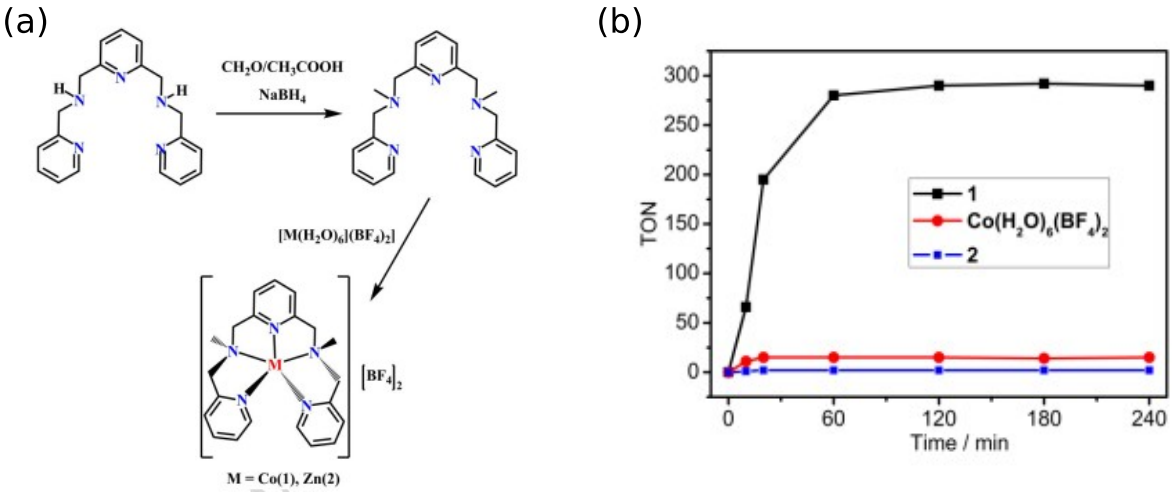

Figure 7: (a) Schematic representation of given complexes, M=Co (1) and M=Zn (2). (b) Hydogen production activities of $[M(Py^{Me}pam)](BF_4)_2$ complexes as well as $Co(H_2O)_6(BF_4)_2$, under same conditions (Song et al., 2017).

A study on H_2 production performance of $Co(bPy)_2(CO)_2$ comprising bi-pyridyl and di-ketone groups in planar plane have performed by (Joliat-Wick et al., 2018). They examine reaction rate of $Co(bPy)_2(CO)_2$ under optimum conditions and it has been found as the catalyst can produce 60 nmol H_2/s. Nevertheless, the role of ketone groups within the catalyst ligand have not been discussed.

The Co(II/I) reduction potential of $Co(bPy)Py_2$ having distorted tetradentate coordination and one bi-pyridyl and two mono pyridyl groups in this structure has been evaluated as -1.11 V by (Guttentag et al., 2013). According to the results, $CoPy_5$, $Co(bPy)_2Py$, and $Co(bPy)Py_2$ possess 1200, 1400, 9000 TONs (H_2/Co), respectively. They concluded that the number of pyridyl ligands in the structure, arrangement and structural geometry are effective for the catalytic activity (Bachmann et al., 2013; Guttentag et al., 2013; Khnayzer et al., 2014).

However, the reason and connection between ligand structure and catalytic performances have not been resolved.

(Tong et al., 2014) have investigated TOF of Co(tPy)(bPy)Py catalyst which owns tri-pyridyl and bi-pyridyl ligands around the Co center. It is demonstrated that associated with Ru based photon absorber molecule, in low concentration, Co(tPy)(bPy)Py shows 586 TOF per hour. However, the mechanism of H_2 production and rate controlling steps have not been explained.

(Varma et al., 2013) have published a study on H_2 production using homogeneous photocatalytic systems. They performed the experiments under visible light irradiation in water using a noble-metal free catalyst, $[Co^{III}(CR)Cl_2]^+$, abbreviated as Cat1, see Figure 8-(a). A comparison of activities between the novel metal-free $[Co^{III}(CR)Cl_2]^+$ catalyts and three different H_2 evolving catalysts such as, [Co{(DO)(DOH)pn}Br_2] abbreviated as Cat2, $[Co(dmbpy)_3]Cl_2$ (Cat3) and $[Rh(dmbpy)_2Cl_2]Cl$ (Cat4) has been established, see Figure 8-(b)-(c)-(d). The experiments carried out under the same conditions shows that H_2 evolving activity of Cat1 is higher than Cat4, even though Cat1 is a noble-metal-free catalyst as well as, cobalt catalysts Cat2 and Cat3 show less activity than Cat1, see Figure 8-(e). It is emphasized that the higher catalytic performance observed for the Cat1 likely depends on the low-valent Co^I oxidation state. A detailed mechanistic perspective for the catalysts under consideration has been given in the study.

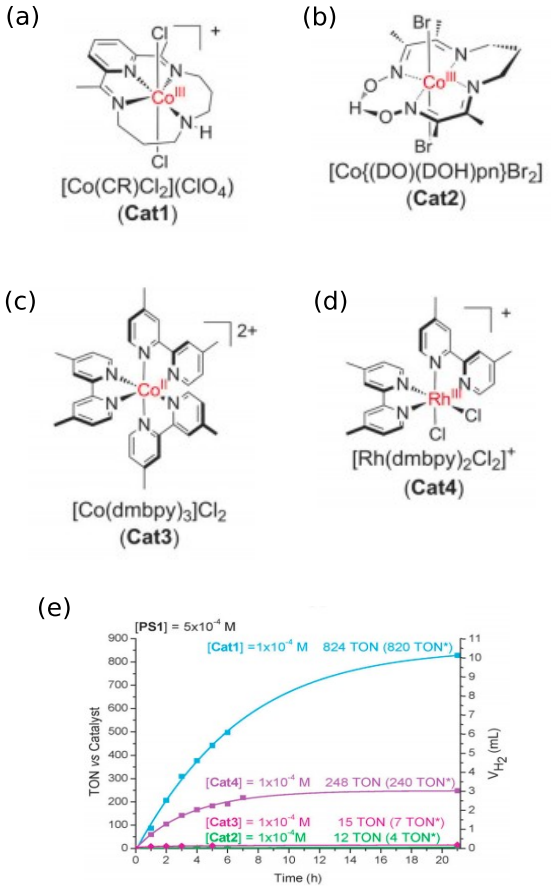

Figure 8: Structure of (a) $[Co^{III}(CR)Cl_2]^+$, (b) $[Co\{(DO)(DOH)pn\}Br_2]$, (c) $[Co(dmbpy)_3]Cl_2$, (d) $[Rh(dmbpy)_2Cl_2]Cl$ catalysts. (e) In the presence of $5x10^{-4}$ mol L^{-1} $[Ru(bpy)3]^{2+}$ as a photosensitizer (PS), H_2 evolving activity (TON) of given catalysts at $1x10^{-4}$ mol L^{-1} versus time are given (Varma et al., 2013).

By combining experimental and theoretical studies, H_2 production mechanism of $Co(bPy)_2Py$ have been investigated by (Smolentsev et al., 2018). An answer has been seeked for the role of mono pyridyl group of the catalyst following the first reduction step. By employing DFT simulations, they modeled all three probable structural models of catalysts under vacuum and the results have been compared with X-ray Absorption Near Edge Structure (XANES). It is inferred from the results that when the mono pyridyl group is dissociated from the Co center, protons can bind to freely moving N atom of the pyridyl ligand implying that pyridyl group is treated as proton donor.

At another study carried out by (Leung et al., 2012) a trans-$CoPy_4$ molecule having four pyridyl groups and planar symmetry has been investigated. Along with -0.6 V onset potential $CoPy_4$ molecule catalyzes the water reduction reaction and its performance has been found as

1150 TONs H_2/Co. However, a mechanistic study on the reaction intermediates have not been performed.

(Gurdal & Iannuzzi, 2020) theoretically studied H_2 production cycle of differently ligated tetra (CoaTPy) and penta-pyridyl (CoaPPy) cobalt-based catalysts possessing distorted octahedral coordination, see Figure 9-(c) and (f). ECEC mechanism of the H_2 production reaction in explicit water environment has been investigated by applying Ab Initio Molecular Dynamics and Density Functional Theory. The oxidation states, Co^{II}, Co^{I}, $Co^{III\text{-}H}$ and $Co^{II\text{-}H}$ have been modeled and solvent response, the role of pyridyl coordination around Co center, the intermediate states of the reaction, their stabilities, as well as reduction free energies have been determined. Solvent and catalyst responses at each intermediate steps of the ECEC mechanism have been addressed. The reduction free energy of the first reduction reaction has been calculated more positive for the CoaTPy with respect to the CoaPPy. The Ab-initio MD trajectories suggest that the Co center of the CoaTPy is more accessible to the water molecules with respect to the CoaPPy which are depicted in Figure 9-(a)-(b)-(d) and (e) where the distances between Co center and the closest water molecules are given and which might explain the higher catalytic activity of the CoaTPy observed experimentally.

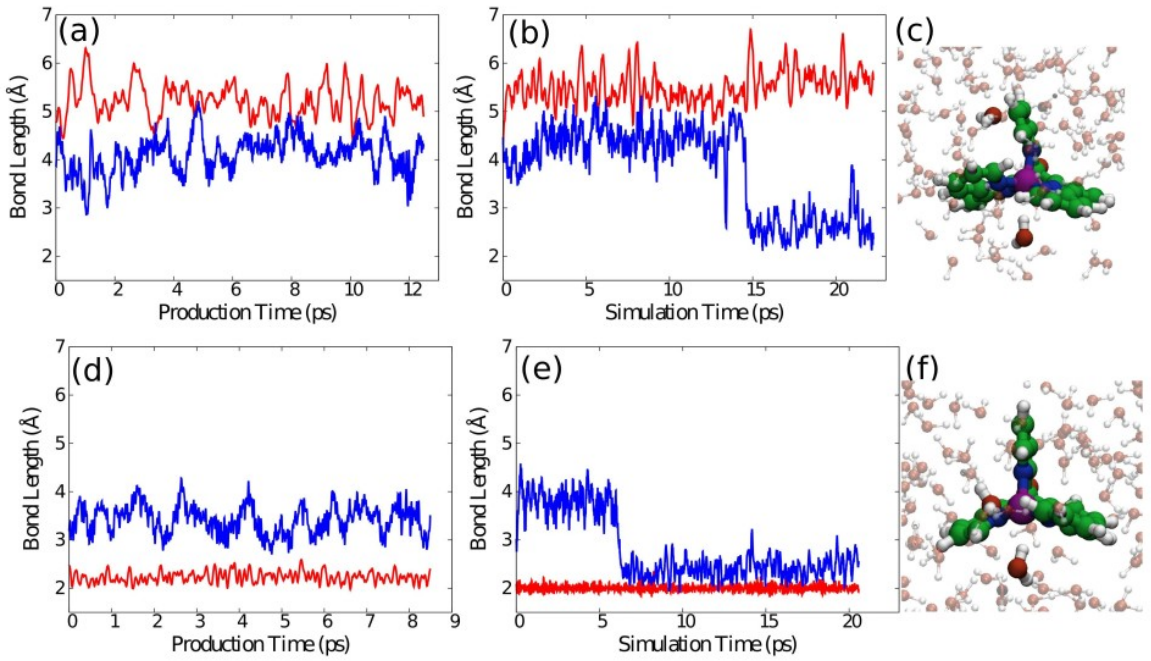

Figure 9: Distances between closest water molecules and Co center of (a) $^{3}(CoaPPy)^{+1}$, (b) $^{1}(CoaPPy)^{+1}$, (d) $^{3}(CoaTPy)^{+1}$, and (e) $^{1}(CoaTPy)^{+1}$ versus simulation time (ps) and the representations of (c) $^{1}(CoaTPy)^{+1}$ and (f) $^{1}(CoaTPy)^{+1}$. Snapshots are taken from the AIMD runs of first electron injection step (Gurdal & Iannuzzi, 2020).

The recent studies demonstrate that the information available in literature is deficient in detail mechanistic understanding of H_2 production using Co based poly-pyridyl catalysts. In order to fill this gap in the literature, in this thesis we theoretically investigate both ECEC and EECC H_2 production mechanism of $CoPy_5$ catalyst, having five pyridyl ligands and perfect octahedral coordination around the Co center. We aim to model all intermediate steps of the reaction as well as different Co spin multiplicities for the same intermediate step in order to shed light on the possible H_2 production mechanism as well as the effects of pyridyl ligands and perfect coordination around the Co center on the proceeding of the reaction.

3 MATERIALS AND METHODS

3.1 **Theory**

The aim of this chapter is to provide a brief explanation on Ab-initio Molecular Dynamics (AIMD) and Density Functional Theory (DFT) simulations, which are employed throughout this thesis. Following, the details of the computational settings have been provided.

3.1.1 **Density Functional Theory and Ab-Initio Molecular Dynamics**

Hohenberg, Kohn and Sham developed Density Functional Theory (DFT) (Hohenberg & Kohn, 1964; Kohn & Sham, 1965) in 1964 in order to calculate electronic structures of the systems. A wavefunction, Ψ, is a formalism which includes information about electrons around a nucleus. DFT, on the other hand, while sharing the similar idea, proposes to use electron density, ρ, instead of complex wavefunction consists of N-electrons (Islam & Kaya, 2018). Basically, electron density identifies the electronic interactions in a non-complex way and correspondingly, the new approach solves the ground state energy of the systems by demanding less computational effort. For ground state energy, the following formulation is introduced, see equation 1 (Cohen et al., 2012).

$$E[\rho]=T_s[\rho]+V_{ne}[\rho]+J[\rho]+E_{xc}[\rho] \qquad (1)$$

The terms given above are called as functionals which are depend on electron density, ρ, corresponding to number of electrons per unit volume. The term $T_s[\rho]$ exemplifies kinetic energy of the non-interacting electrons for Kohn-Sham system, $V_{ne}[\rho]$ includes all potential energy arises from nucleus-electron interactions, $J[\rho]$ classical repulsion energy of electrons between each other. The remain term named as exchange-correlation functional, $E_{xc}[\rho]$, introduces the non-classical interactions between electrons and its exact

formulation has not been available (Cohen et al., 2012). Electron correlation stands for the interaction between an electron and remain electrons within a molecule or atom. Fermion particles practice an electron exchange between each other, this situation addresses by electron exchange within the term exchange-correlation (Gritsenko et al., 1997).

The alternative expression of the exchange-correlation term is given in equation 2. At the given equation, $T_e[\rho]$ is many-body kinetic energy and $V_{ee}[\rho]$ represents non-classical electrostatic interactions. As it is mentioned, exact formulation of the exchange-correlation functional is unknown, thus in order to apply DFT properly, an appropriate formulation should employed. Therefore, with accomplishment of high accuracy, a variety of approximations have been introduced (Orio et al., 2009).

$$E_{xc}[\rho]=(V_{ee}[\rho]-J[\rho])+(T_e[\rho]-T_s[\rho]) \quad (2)$$

One of the previously used approximation is local-density approximation (LDA), which is only based on electron density. Generalized Gradient Approximation (GGA) is one of the most popular approximations introduced for exchange correlational functional. It has a different point of view which combines electron density as well as electron gradient in order to include effects of inhomogeneity of electron distribution appertain to molecular orbitals and it is shown to achieve better approximations than LDA (Orio et al., 2009). Some generally used GGA functionals are Perdew-Burke-Ernzerhof (PBE) (Perdew et al., 1996) and Becke exchange/Lee-Yang-Parr exhange-correlation (BLYP) functional (C. Lee et al., 1988). These functionals find to be less accurate for transition metal based molecules compared to alkali metals (IA) or alkaline earth metals (IIA). In order to overcome accuracy concerns of PBE and BLYP, hybrid density functionals have been introduced, which employ GGA and Hartree-Fock method together (Orio et al., 2009; Skorodumova et al., 2001). PBE0 (Ernzerhof & Scuseria, 1999) and HSE06 (Heyd et al., 2003; Krukau et al., 2006) are the most commonly used hybrid functionals. It is shown that affirmative results have been achieved through using these hybrid functionals, moreover, the improvement for estimating band gaps of semiconductors as well as better representation of transition-metal oxides have been observed using hybrid functionals (Morin & Pelletier, 2013).

The dispersion interactions occur between non-bonded subsystems have been remain unidentified resulting from incompleteness of the mentioned functionals. Therefore, simulations for certain systems where physical interactions are crucial omitting dispersion interactions might result in obtaining incorrect behavior of the systems. In order to prevent this deficiency of DFT, including a term for empirical dispersion energy correction is the most commonly used approach. (Grimme et al., 2010) proposed an empirical dispersion energy correction term which assigns parameters to each kind of atom and updates at each simulation step. Non-local van der Waals (vdW) density functionals, on the other hand, have been introduced as an alternative method for improving the description of dispersion interactions already within self consistent field cycles of the DFT. Vydrow-Voorhis (rVV10) (Sabatini et al., 2013; Vydrov & Van Voorhis, 2009) is one of the most used non-local vdW density functionals. Indeed, in this thesis Co-based penta-pyridyl catalyst reaction mechanism in water has been investigated using PBE exchange correlational functional together with rVV10 vdW functional. Besides, detailed electronic structure analysis of the selected configurations and calculations of the reduction free energies have been carried out using PBE0/rVV10 density functional.

Ab-Initio Molecular Dynamics (AIMD) simulations can enable one to study configurational rearrangements under realistic experimental conditions by sampling phase space trajectories. Considering Born-Oppenheimer Approximation (Barnett & Landman, 1993), the electronic effects are calculated through quantum mechanical principles and electrons of atoms at the system hypothesized that they synchronously accord with atomic rearrangements. Accordingly, for each step of the MD simulation, nuclear motion and electrons considered separately due to the assumption of fixed nucleus, when compared the weight of electrons with nucleus, nuclei is much heavier than electrons and as a result, the movement of nuclei is much more smaller than electrons. Consequently, forces of electronic calculations give rise to propagation of nuclei from one time step to the next. We apply AIMD simulations in order to model each intermediate step of both EECC and ECEC H_2 production mechanisms.

3.2 **Computational Methodology**

We perform Ab-Initio Molecular Dynamics simulations (Marx & Hutter, 2019) in order to model each intermediate step of the H_2 production. Open source CP2K simulation package have been used in all simulations (Kühne et al., 2020). PBE density functional (Perdew et al., 1996) in general gradient approximation (GGA) formalism is employed for AIMD simulations. Goedecker-Teter-Hutter (GTH) potentials are applied for the estimation of core electron interactions with the valence shell and nucleus (Goedecker et al., 1996). Therewithal, valence electrons of the atoms are modeled explicitly and valence shells of Co, N, C, O and H contain 17, 5, 4, 6 and 1 electrons, respectively. DZVP-MOLOPT basis set is used for all atomic kinds (VandeVondele & Hutter, 2007). For auxiliary plane wave basis set, a cutoff of 400 Ry utilized. Dispersion interactions are taken into consideration by (Sabatini et al., 2013) proposal, applying Vydrov and Van Voorhis, in the revised form formalism (rVV10). It is shown that the empirical short range interactions of rVV10 density functional parameter estimates the hydrogen bond structure for water molecules more accurately, thus, set to 9.3 (Ambrosio et al., 2015). Periodic boundary conditions and spin polarizations are always applied.

For CoPPy complex, AIMD simulations are carried out in a box defined as cubic with explicit water environment. The CoPPy catalyst first solvated in 215 water molecules and the simulation volume is relaxed by performing AIMD simulations for approximately 20 ps in the isothermal-isobaric ensemble (NPT). Simulations box volume is determined as 6163.28 $Å^3$. Edge length of cubic ensemble simulations obtained as 18.33 Å. Following the determination of the simulation box size, each intermediate step modeled by applying AIMD simulations in the canonical ensemble (NVT) for approximately 20 ps. Time step is set to 0.5 fs. Canonical sampling through velocity rescaling (CSVR) (Bussi et al., 2007) thermostat with a time constant of 100 fs is applied in order to keep the simulations temperature at 300 K.

DFT is a method frequently used in literature, in order to optimize geometric structures of molecules, establish minimum energy configurations, interaction energies, electron band gaps, molecular orbital distributions and so on (Gurdal et al., 2015, 2017; Gurdal & Iannuzzi, 2017). In this thesis, Density Functional Theory (DFT) calculations have been applied to selected AIMD snapshots of reaction intermediate steps and the electronic structure alterations of each intermediate steps are calculated using PBE0/rVV10 hybrid density

functional (Ernzerhof & Scuseria, 1999). The same approach is also used for calculating reduction free energies of the reduction steps of both EECC and ECEC mechanisms by applying free energy perturbation theory. PBE0 Hartree-Fock exchange fraction parameter is used as 0.25.

3.3 **Catalytic Cycle for H_2 Production**

In this thesis, in order to achieve water reduction, a heterolytic H_2 production mechanism has been employed. The catalytic reaction pathway depicted in Figure 10-(a) and 10-(b) which shows the Co spin multiplicities and charges along the ECEC and EECC pathways. According to the literature search, there is a limited knowledge on the heterolytic hydrogen (H_2) production mechanism, ECEC and EECC, is available. ECEC and EECC are the probable H_2 production reaction mechanisms and E and C stand for electron transfer and chemical step, respectively. Both mechanisms consist of subsequent electron and proton transfers to the reaction center which includes in total 2 electron and 2 proton transfers (Behnke et al., 2018).

Co based penta-pyridyl ligand having octahedral arrangement owns quartet spin multiplicity at the initial state of the reaction. The initial charges of the catalyst system owns +2 charge. Under normal conditions, neutral Co atom has an electron configuration corresponding to "[Ar]$3d^7 4s^2$". At the given mechanism, the initial state Co(II) has "[Ar]$3d^7$" electron configuration. Following the first electron injection, Co(I) is formed which has "[Ar]$3d^8$" electron configuration (Basu et al., 2016; Rodenberg et al., 2015). Accordingly, for the following step, two expectative spin states for Co would be singlet or triplet. For both ECEC and EECC mechanism, both triplet and singlet spin states are modeled in order to determine the most probable spin state of the catalyst that undergo the first protonation (ECEC) or the second electron injection (EECC). At the ECEC mechanism, following the first protonation electron configuration of the Co at the Co(III)-H hydride becomes "[Ar] $3d^6$". Accordingly, at this state, the possible spin multiplicities of the Co(III) are known as quintet, triplet and singlet. It is a known fact that Crystal Field Theory takes an important place for specifying systems which includes transition metals and ligands. In the literature, there are several studies which states that the pyridine ligands create a strong ligand field around the transition metal centers. According to this, the energy levels between d orbitals of the transition metals

is high at molecules which contains pyridine ligands and in parallel with this, transition metal owns low spin multiplicity (Huheey et al., n.d.; Pal, 2018). Consequently, at this study quintet spin state for Co(III)-H intermediate step is neglected.

In this thesis, each intermediate steps of the ECEC and EECC H_2 production reaction mechanisms have been simulated. As it is mentioned above, the first step of both mechanisms results in two different spin multiplicities, triplet or singlet spin state, with a charge of +1. The simulations for both spin states are carried out in order to determine the appropriate spin state for the next step which is the first protonation for the ECEC or the second electron injection for the EECC mechanism. Following the second electron injection at the ECEC mechanism and first protonation for the EECC mechanism, the catalyst can have doublet or quartet spin states and a charge of +1. Both spin states have been modeled in order to determine the most appropriate spin state, depending on various traits e.g., potential energy, stability, that should be employed for the second protonation for both mechanisms. Following the second protonation, H_2 production cycle is completed and diffusion of the H_2 to the solvent environment should be observed, see Figure 10-(c) and (d), respectively.

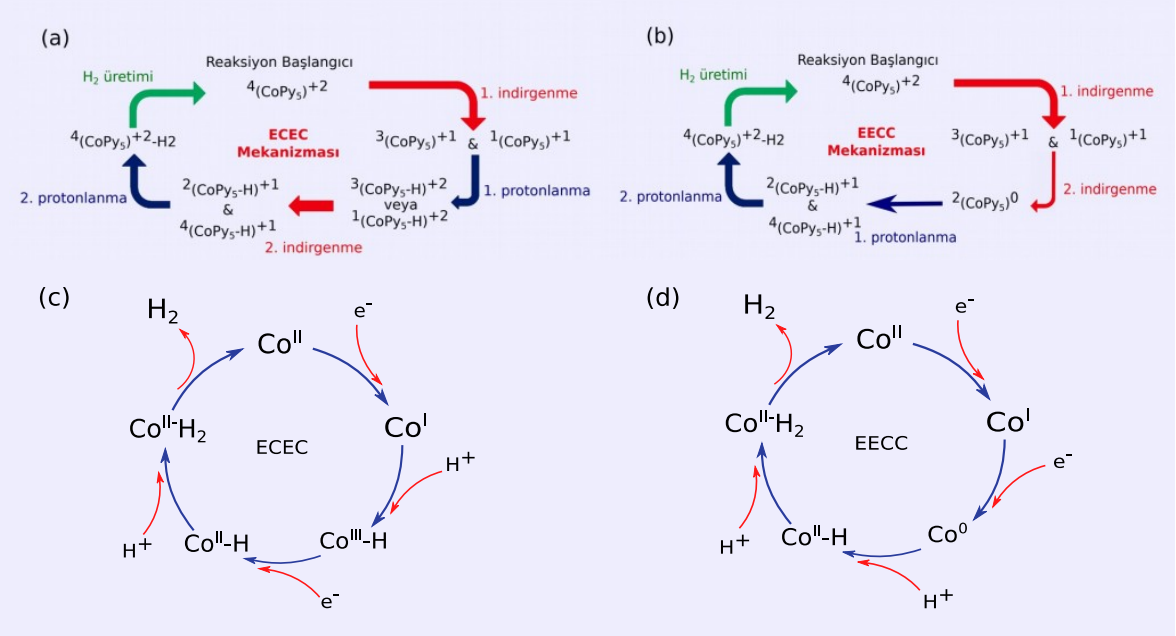

Figure 10: (a) Visual representations of the ECEC and (b) EECC reaction mechanisms for $CoPy_5$. At each given step, the number (m) on the left hand side of the parenthesis indicates the spin multiplicity of the system, while the number on the right hand side (n) indicates the total charge of the system, $^{m}(CoPy_5)^{n}$. Co(II) shows the initial state of the catalyst, while (c) Co(III)-H hydride is formed in the ECEC mechanism, (d) Co^0 is formed in the EECC mechanism (Gurdal & Iannuzzi, 2020).

3.4 $CoPy_5$ Catalyst Under Consideration

$CoPy_5$ is composed of poly-pyridyl ligand consists of five pyridyl groups connected to each other via -OH groups and has got an perfect octahedral shape as shown in Figure 11-(a)-(b). $CoPy_5$ provides one coordination site for water molecules to bind to the Co center. It is experimentally shown that as a water reduction catalyst, $CoPy_5$, preserves its stability during the reaction.

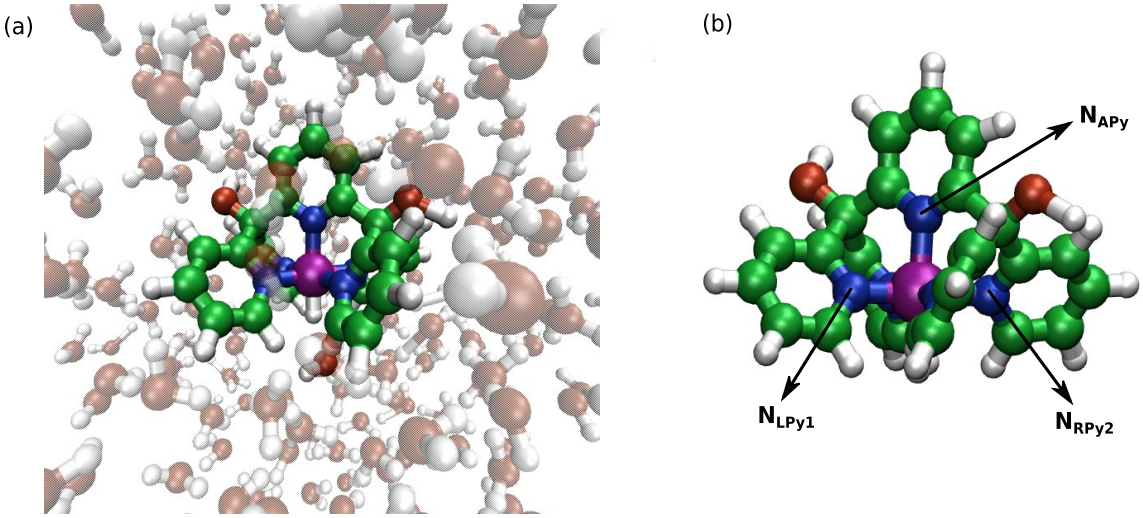

Figure 11: (a) Ball and stick representation of cobalt based penta-pyridyl water reduction catalyst having octahedral arrangement, $CoPy_5$ in water. Green balls represent C, white: H, purple: Co, blue: N, red: O. (b) Pyridyl rings named with connected N atoms as N_{APy}, N_{RPy2} and N_{LPy1}.

4 RESULTS AND DISCUSSIONS

The geometry optimization of the $CoPy_5$ water reduction catalyst has been carried out under vacuum by performing DFT and PBE/rVV10 density functional. Spin multiplicity of the $CoPy_5$ catalyst is identified as 4 and total charge is +2, $^4CoPy_5^{+2}$. Following the geometry optimization, the catalyst is solvated in 215 water molecules in order to mimic solvent environment during the H_2 production reaction. The volume of the catalyst/water system is relaxed by performing AIMD simulations in the isobaric-isothermal (NPT) ensemble for 20 ps. The total number of atom is 700, pressure is 1 atm and simulation temperature is set to 300 K. As it is depicted in Figure 12, potential energy and temperature of the system shows small fluctuations at the production phase of the simulation. From the AIMD-NPT simulations the cubic simulation volume is determined as 6163.28 $Å^3$. Following, we first summarize the results of the ECEC reaction mechanism and we then proceed with the analysis of the EECC reaction mechanism.

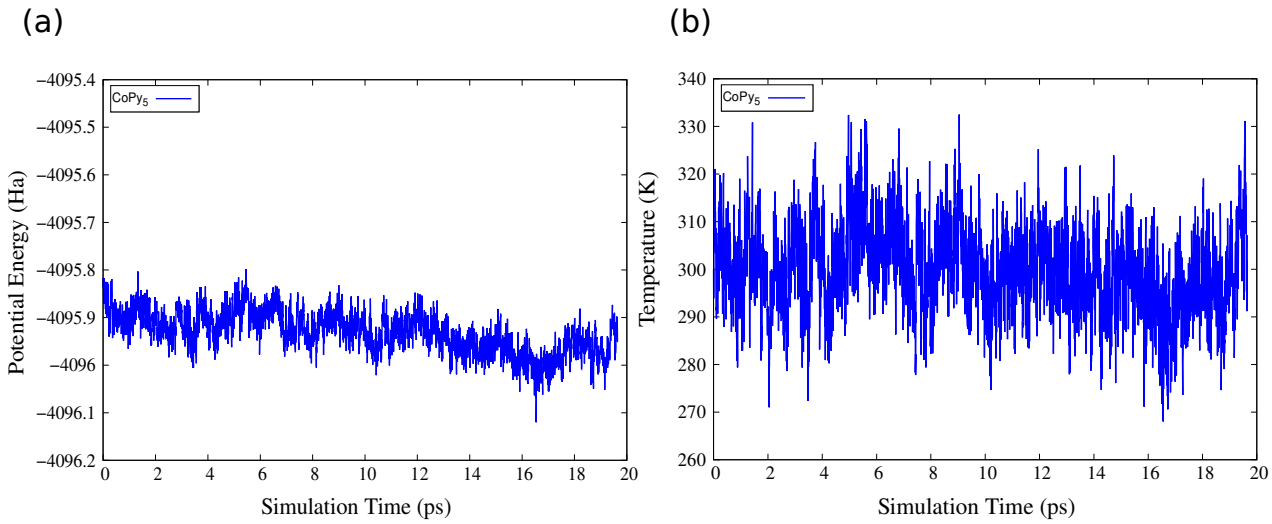

Figure 12: (a) Potential energy and (b) Temperature alteration over the AIMD-NVT simulation for the $CoPy_5$ catalyst at the initial state, multiplicity 4 and charge +2, $^4(CoPy_5)^{+2}$.

4.1 Intermediate Steps of the ECEC Reaction Mechanism

As it is mentioned previously, the initial states of the $CoPy_5$ owns 4 as spin multiplicity and AIMD simulations in the canonical ensemble (NVT) have been carried out to simulate initial state of the catalyst in explicit water environment. The snapshots obtained from the AIMD-NVT trajectories are depicted in Figure 13-(a) and Figure 13-(c). Water molecules disperse around the water reduction catalyst homogeneously. As depicted in Figure 13-(b), one water molecule binds to Co center of the catalyst which is labeled as O_{wat1}. The one another water molecule is labeled as O_{wat2} which represents the other water molecule situated around Co center and provides coordination above the Co. The distance between the Co center and O_{wat1} fluctuates around 2.1 Å and distance between Co center and O_{wat2} is measured as 4.3 Å which is a relatively long distance. The distances between N atoms within the ligands of the $CoPy_5$ and Co center are demonstrated in Figure 13-(d). Distances fluctuate around 2.1 Å and during the simulation bond dissociation between the ligands and the Co center have not been observed.

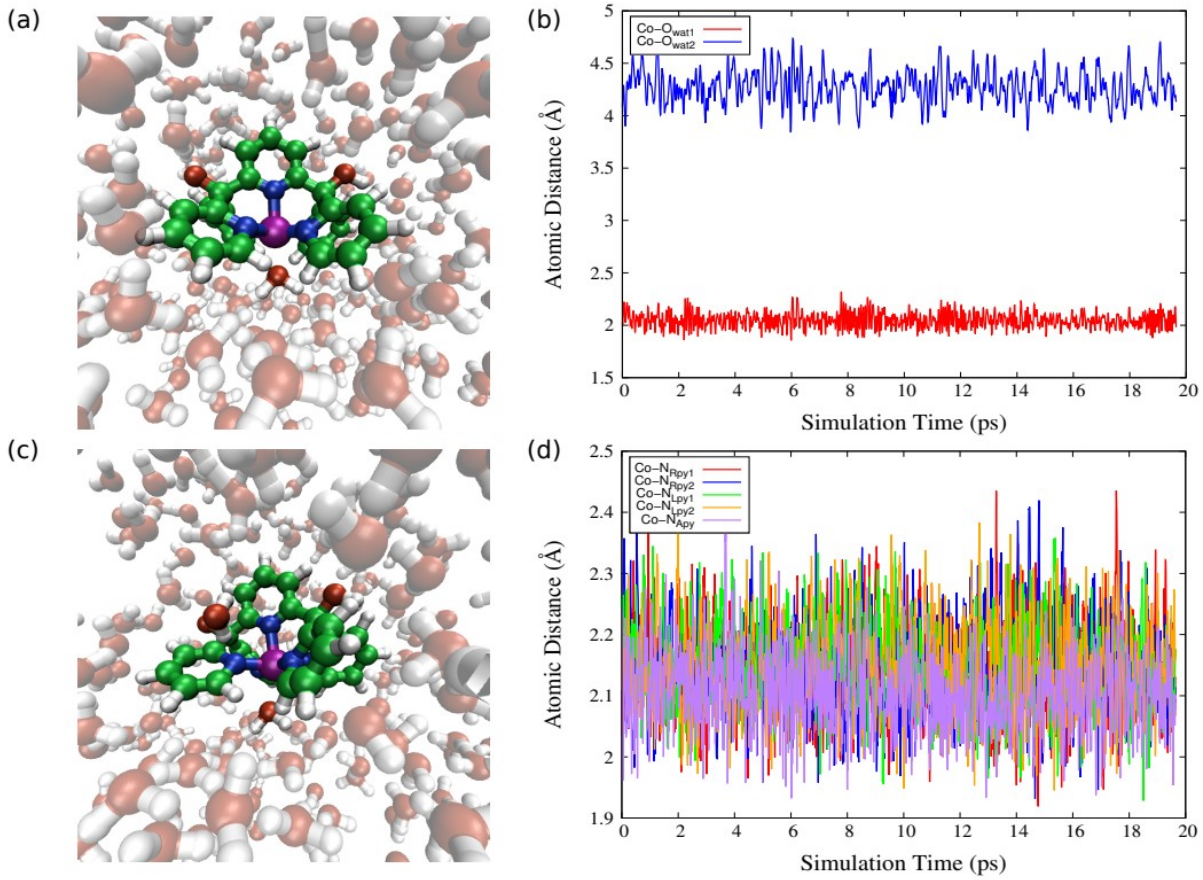

Figure 13: (a) A snapshot provided from AIMD-NVT simulation for the initial state, $^{4}(CoPy_5)^{+2}$. (b) Fluctuations of Co and O of water molecules over the simulation. (c) The two closest water molecules to the Co center. (d) Fluctuations of Co and surrounding N atoms over the simulation

The first step of both ECEC and EECC reaction mechanisms is the first electron injection in which the system is reduced by gaining an electron. Along with the first electron injection, the charge of the system changes as +1 and as depicted in Figure 10-(a)-(b), the catalyst can have singlet or triplet spin multiplicities. We continue our simulations by injecting one electron to the system and model the first reduction step of the catalytic cycle. We simultaneously run two AIMD-NVT simulations having triplet and singlet spin states.

Figure 14-(a) demonstrates a snapshot of the triplet spin state obtained after the first electron injection to the system. The simulations are carried out for 17.55 ps and potential energy of the system is preserved as well as temperature of the system which is fluctuating around 300 K. The O of the closest water molecule, O_{wat1}, preserves its distance to the Co center along the AIMD-NVT trajectory and Co-O_{wat1} bond dissociation have not been observed. H atoms of two different water molecules approach to the reaction center from top of the catalyst,

specified as H_{wat2} and H_{wat3}. As it is depicted in Figure 14-(b), the closest water molecule, O_{wat1}, occupy its place in the simulation box having a fluctuating distance around 2.1 Å to the Co center. Therebeside, distances between Co and the second closest water molecule, Co-O_{wat2}, and the third closest water molecule, Co-O_{wat3} fluctuate widely around 4 Å. The coordinations between H atoms of the water molecules, H_{wat2} and H_{wat3}, and Co center of the water reduction catalyst are depicted at Figure 14-(c) and 14-(d). Distance of Co-H_{wat2} decreases from 4.5 Å to 3 Å and as simulation continues the distance again increases to 4.5 Å and decreasing again periodically. The reason is that H_{wat2} is rotating during the simulation and is providing a coordination with the reaction center and with the solvent. The atomic distances of Co-H_{wat2} is on the decline until 2.5 Å in conjuction with the simulation time increasing to 17 ps. The distance between Co-H_{wat3}, on the other hand, has large fluctuations around 5.2 Å up to 14 ps of the simulation time compared to Co-H_{wat2} distance. As simulation time reaches around 18 ps, the average Co-H_{wat3} distance becomes around 4.7 Å.

As a summary, for the triplet spin state we have not observed any conformational change for the O_{wat1} which is very structured in the close vicinity of the reaction center. Previous simulations carried out for the triplet spin state of the CoTPy and CoaPPy catalysts also do not show rotation of the closely coordinated water molecule even though CoTPy and CoaPPy have distorted octahedral geometries and in the vicinity of the Co center they provide more open structures with respect to $CoPy_5$ (Gurdal & Iannuzzi, 2020).

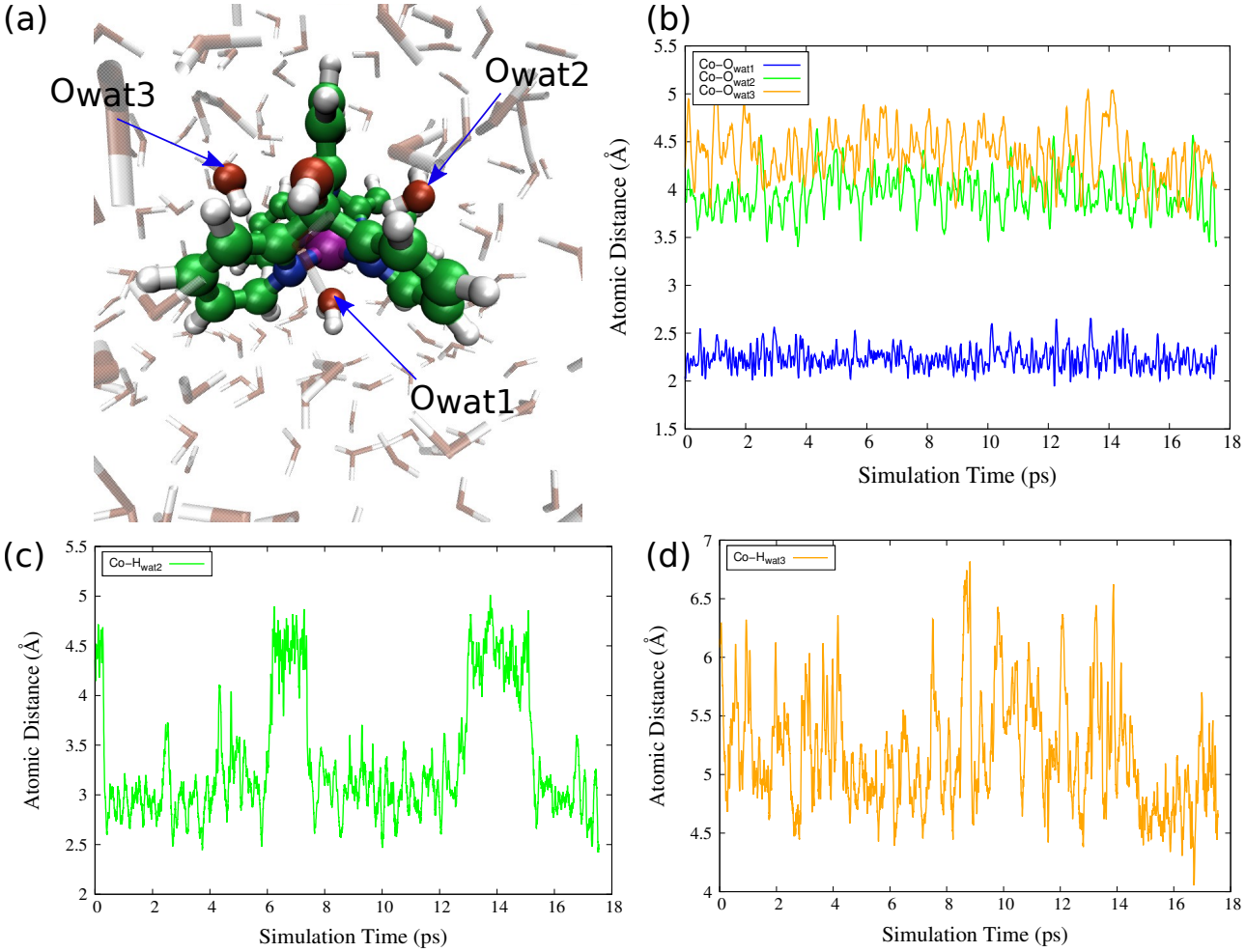

Figure 14: (a) Snapshot taken from the AIMD-NVT simulations of the triplet spin state $^{3}(CoPy_5)^{+1}$ at 18 ps of simulation time (b) Alterations along the simulation for distances between O of the closest three water molecules and Co center of the catalyst (c) Fluctuations of distances between Co center and H of second closest water molecule (H_{wat2}) as well as (d) Co center and H of third closest water molecule (H_{wat3}).

The illustrations of singlet spin state of the first electron injection are provided at Figure 15-(a). The first notable feature is that the water molecule, O_{wat1}, which previously provided a close coordination with the Co center changes its conformation shortly after the beginning of the simulation and enables the Co-H^+ bond. Along with the electron injection to the Co center, strength of the interactions between Co and O_{wat1} decreases and the proton of the water molecule binds (H_{wat1}) to more negative Co center. In addition to this, H of the other water molecule, H_{wat4}, approaches to the reaction center. The distance between Co-O_{wat1} established as 2 Å at the beginning of the simulation increases to 3.2 Å along with new Co-H_{wat1} bond

formation, see Figure 15-(b). The distance between Co-H_{wat1} decreases from 4.5 Å to 2 Å due to the conformational change related to the Co-H_{wat1} bond formation, see Figure 15-(c).

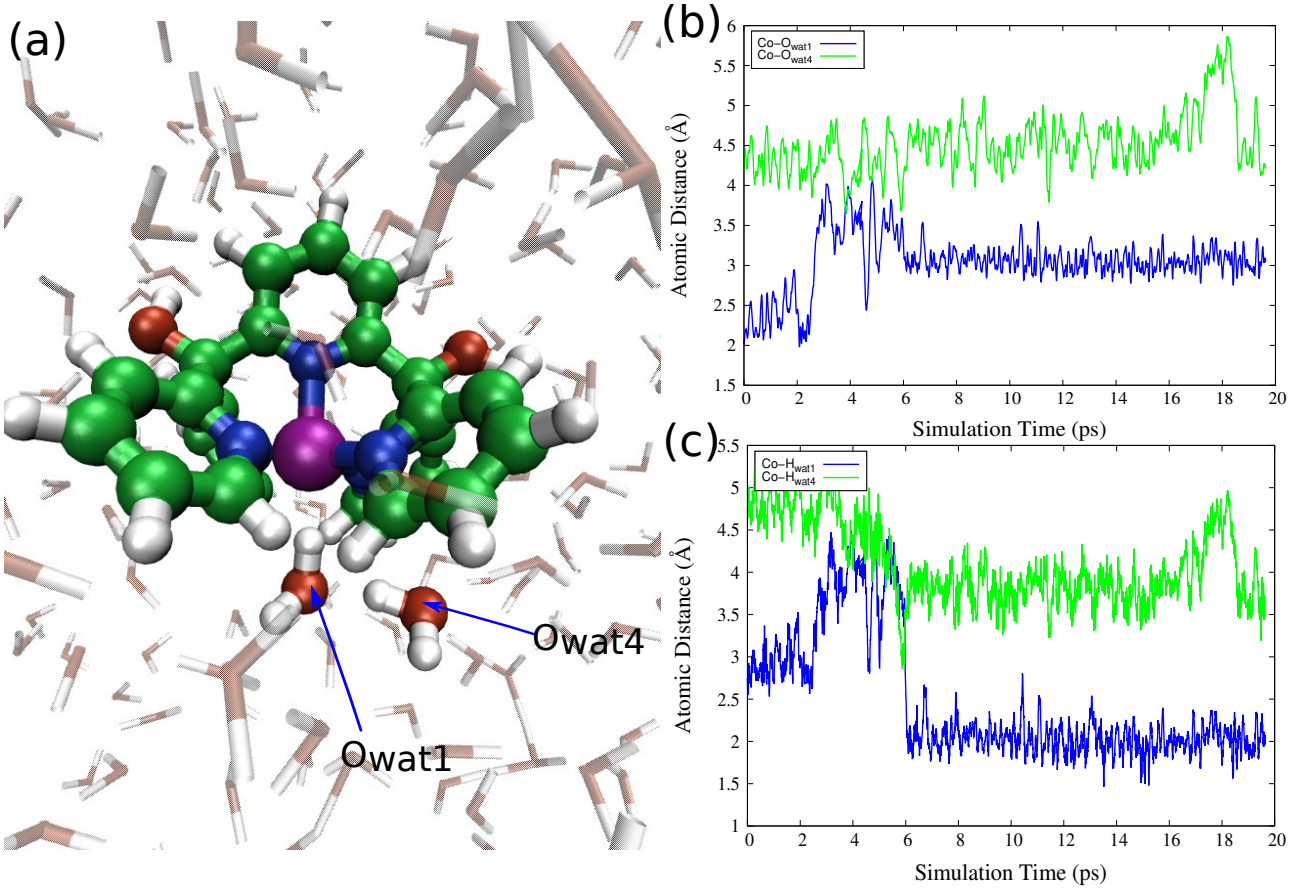

Figure 15: (a) Snapshot taken from the AIMD-NVT simulations of the singlet spin state $^{1}(CoPy_5)^{+1}$ at 19.63 ps of simulation time (b) Alterations along the simulation for distances between O of the closest two water molecules and Co center of the catalyst (c) Fluctuations between Co center and H atoms of the two closest water molecules.

These results demonstrate that the singlet spin state model which is a follow up of the first electron injection leads to a bond formation between Co-H_{wat1}. Previous simulations carried out for the singlet spin state of the CoTPy and CoaPPy catalysts show that the closet water molecule rotates around 5 ps and 15 ps of the simulation time, respectively (Gurdal & Iannuzzi, 2020). For the $CoPy_5$ we observe such kind of rotation at around 6 ps of simulation time. CoTPy and CoaPPy have distorted octahedral geometries and in the vicinity of the Co center they provide more open structures with respect to $CoPy_5$. Besides, CoTPy has only one pyridine and one bipyridine ligand on the equatorial plane which even provides more open structure with respect to CoaPPy, thus obtains water rotation very fast, around 5 ps. We also observe the similar trend for $CoPy_5$ having perfect octahedral coordination. As result of the

simulations carried out simultaneously for both triplet and singlet state of the catalyst the H_2 reaction mechanism of $CoPy_5$ proceeds to the first protonation (ECEC) or to the second reduction (EECC) with singlet spin state.

The second intermediate step of the ECEC mechanism is the first protonation, see Figure 10-(a) and as it is indicated previously, the H_2 production reaction proceeds with singlet spin state. The proton is provided to the Co center from the closest proton of the water molecule, H_{wat1}, and OH^- has been formed in the solvent. In order to preserve the charge of the system, an extra proton added to the simulation box away from the Co center and as a result, a H_3O^+ ion is formed. A snapshot taken from the AIMD-NVT simulation of $^1(CoPy_5)^2$ system is given in Figure 16-(a). The proton binds to Co center taken from the closest water molecule and the distance between Co and proton of the closest water molecule is depicted in Figure 16-(b). In the beginning of the simulation the proton (H_{wat1}) moves towards the OH^- of the same water molecule which gives rise to increased Co-H_{wat1} distance. However, as simulation evolves Co center grabs the proton and Co-H_{wat1} distance becomes around 1.45 Å. As the simulation proceeds, distance of between oxygen atom of the OH^- and proton (H_{wat1}) increases from 1 Å to around 2.5 Å which also implies that the bond between OH^- and the proton of the water molecule dissociates, see Figure 16-(c). At the same time at around 2.5 ps, the proton of the closest water molecule establishes a bond with the Co center of the water reduction catalyst, see Figure 16-(b). The distance between the proton and the oxygen of the OH^-, $O_{wat1,}$ which belong to the same water molecule is very short at the beginning of the simulation meaning the proton is binded to the OH^-. Afterwards, the distance between OH^- and proton increases over the simulation time and the bond between them is broken ultimately. Besides, the remained OH^- forms hydrogen bonding interactions with surrounding water molecules and diffuses to the solvent. The proton, on the other hand, binds to the Co center and remains stable until the end of the simulation. As the results suggest, the proton is supplied to the Co center by the closest water molecule and formed Co(III)-H hydride is stable.

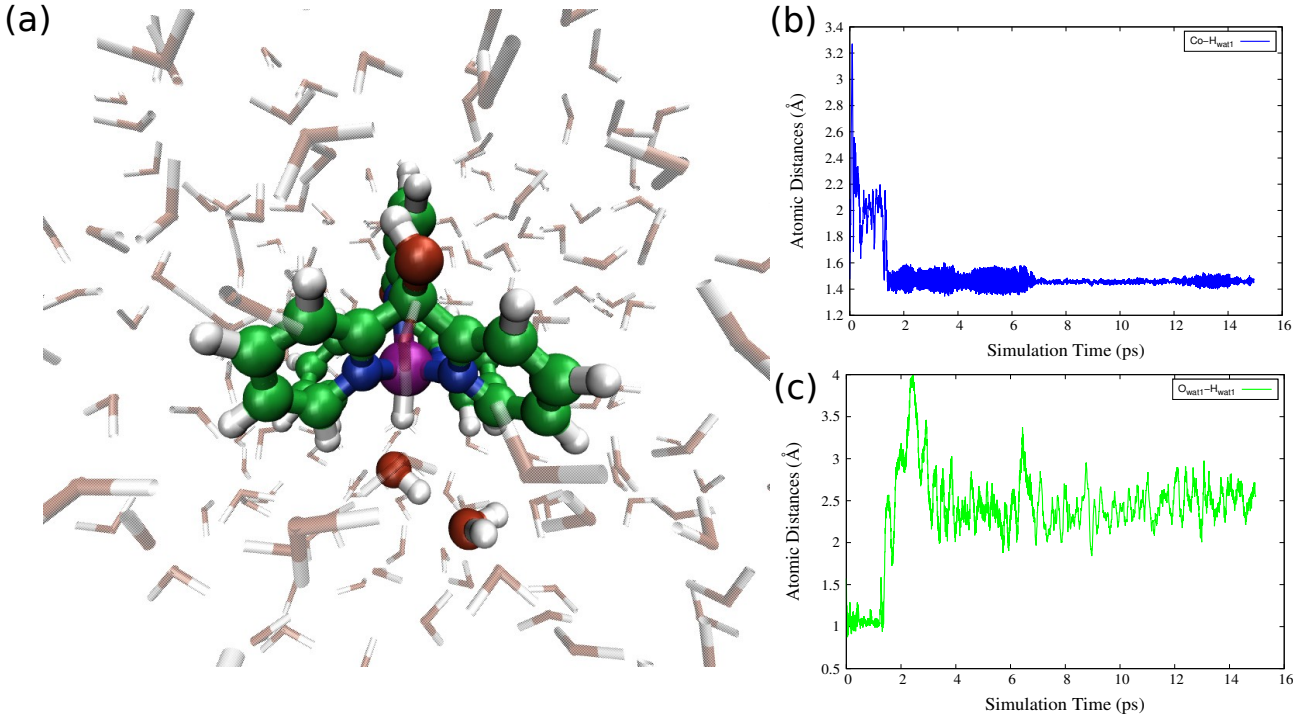

Figure 16: (a) A snapshot taken from AIMD-NVT simulation of the first protonation step, $^{1}(CoPy_5)^{+2}$, at 15 ps of simulation time is given. (b) After first protonation, $^{1}(CoPy_5)^{+2}$, the atomic distance between the Co and the bonded proton supplied by the nearest water molecule (H_{wat1}) is plotted in blue, Co-H_{wat1}. (b) The atomic distance between the OH^- ion and the proton bonded to the Co is plotted in green, O_{wat1}-H_{wat1}.

The next step of the ECEC mechanism is the second electron injection and this intermediate step can proceed either with doublet or quartet spin states. Within our study, we modeled both doublet and quartet spin states for the second electron injection step, see Figure 10-(a). We run our AIMD-NVT simulations for 17 ps. At Figure 17-(a) distances between Co-H^+ and H_{wat1} as well as Co-H^+ and H_{wat2} are plotted along the simulation time for the doublet spin state. Note that here H^+ represents the proton binded to the Co and H_{wat1} and H_{wat2} are the water hydrogens closest to the proton binded to the Co center.

In the beginning of the simulation, the distance between Co-H^+ and H_{wat1} was around 4 Å. As the simulation continues, the mentioned distance decreases until to 1.7 Å. The distance between Co-H^+ and H_{wat2}, on the other hand, increases from 2.4 Å to 3.5 Å. Although, the simulation is continued to 17 ps, the alteration of H_{wat2} and H_{wat1} coordination with Co(III)-H hydride seems to continue. The AIMD-NVT snapshot provided from the trajectory of the second electron injection with doublet spin state is given at Figure 17-(b). From the given results, it can be inferred that the state having doublet multiplicity, only one proton from the

solvent can coordinate with the Co(III)-H hydride. While H_{wat1} is coordinating with the Co-H^+, the other H_{wat2} is interacting with the solvent. As the same vein, while H_{wat2} is coordinating with the Co-H^+, H_{wat1} is interacting with the solvent through hydrogen bonding.

The results of the quartet spin state simulations are depicted in Figure 17-(c) which shows the distances between Co-H^+ and H of the closest water molecule, H_{wat1}, as well as Co-H^+ and the the second closest water molecule, H_{wat2} and at Figure 17-(d) which shows a snapshot taken from the AIMD-NVT trajectory. The distance between Co-H^+ and H_{wat1} first increases from 1.5 Å to 2.5 Å and then decreases from 2.5 Å to around 1.5 Å again and remains stable until the end of the simulation. Simultaneously, the distance between Co-H^+ and H_{wat2} decreases from 3.5 Å to 1.5 Å. These results give a conclusion that both protons of water molecules can provide a coordination with the Co center. Moreover, compared to the doublet spin state, at quartet spin state, both water molecules are willing to provide a proton for the Co center of the catalyst. Due to the fact that, stability of the systems are substantial for our simulations, both doublet and quartet models demonstrate that the H_2 production reaction mechanism is likely to continue with quartet spin multiplicity for the second protonation.

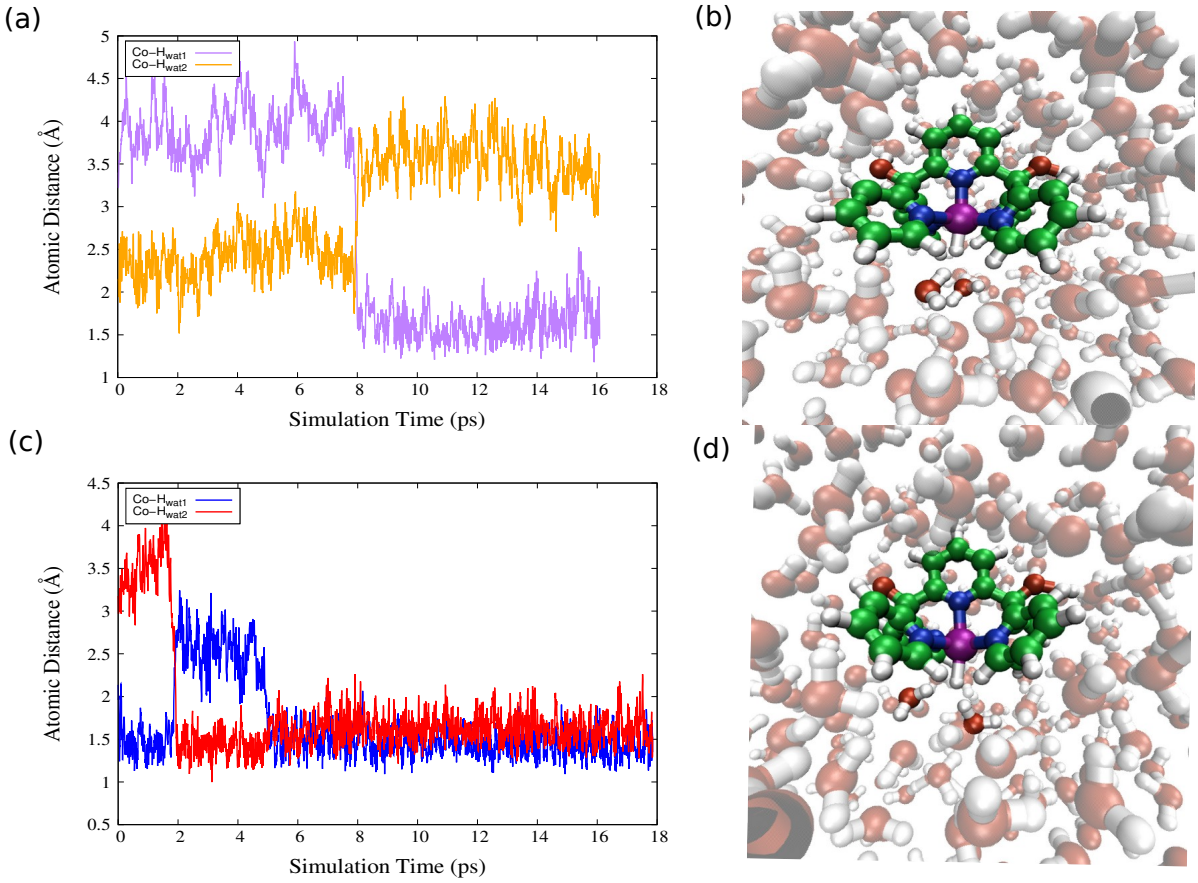

Figure 17: (a) Co-H_{wat1} and Co-H_{wat2} distances along the AIMD for $^{2}(CoPy_5)^{+1}$ which are depicted by purple and orange, respectively, where Co represents Co-H^{+} residue. (b) A snapshot illustrated from AIMD-NVT simulation $^{2}(CoPy_5)^{+1}$ trajectory at 16 ps of simulation time, (c) Co-H_{wat1} and Co-H_{wat2} distances along the AIMD for the $^{4}(CoPy_5)^{+1}$ are depicted by blue and red, respectively, where Co represents Co-H^{+} residue. (d) A snapshot illustrated from AIMD-NVT simulation of $^{4}(CoPy_5)^{+1}$ trajectory at 17 ps of simulation time.

The fourth and last step of the ECEC mechanism at H_2 production system is the second protonation. This step gives rise to production of the H_2 molecule and the multiplicity as well as the charge of the system should, in principle, revert back to the initial state as, $^{4}(CoPy_5)^{+2}$-H_2. Figure 18-(a) implifies the bond distances between H atoms of the H_2 molecule formed at the end of the mechanism. Ideally, the protons should bind to each other and move away from the catalyst. Conformably to the ideal situation, the distances between two hydrogens fluctuates around 0.8 Å and preserves its stability until the end of the simulation, which signifies that the H_2 molecule is, indeed, formed. However, due to the presence of surrounding water molecules and the geometric nature of the catalyst, the formed H_2 molecule struggles with moving away from the Co center and the distance between Co center and the H_2

molecule remains stable at around 1.9 Å, see Figure 18-(b). At Figure 18-(c) a snapshot is provided from the 4 ps of the simulation time. It is still interesting that we could not observe diffusion of the H_2 from the vicinity of the Co center. Previous simulations carried out for CoTPy and CoaPPy already show diffusion of the H_2 molecules in the beginning of the simulation (Gurdal & Iannuzzi, 2020). We continue our simulations in order to see the diffusion of the H_2 molecule to the solvent, however the perfect octahedral coordination of the catalyst and its more closed structure around Co might have an effect on the diffusion of the H_2 molecules. The experimental study showed that H_2 production rate of CoTPy and CoaPPy are higher than the rate obtained by $CoPy_5$ which might be related to the difficult diffusion of H_2 from the reaction center which could also result in delayed next reduction and protonation steps.

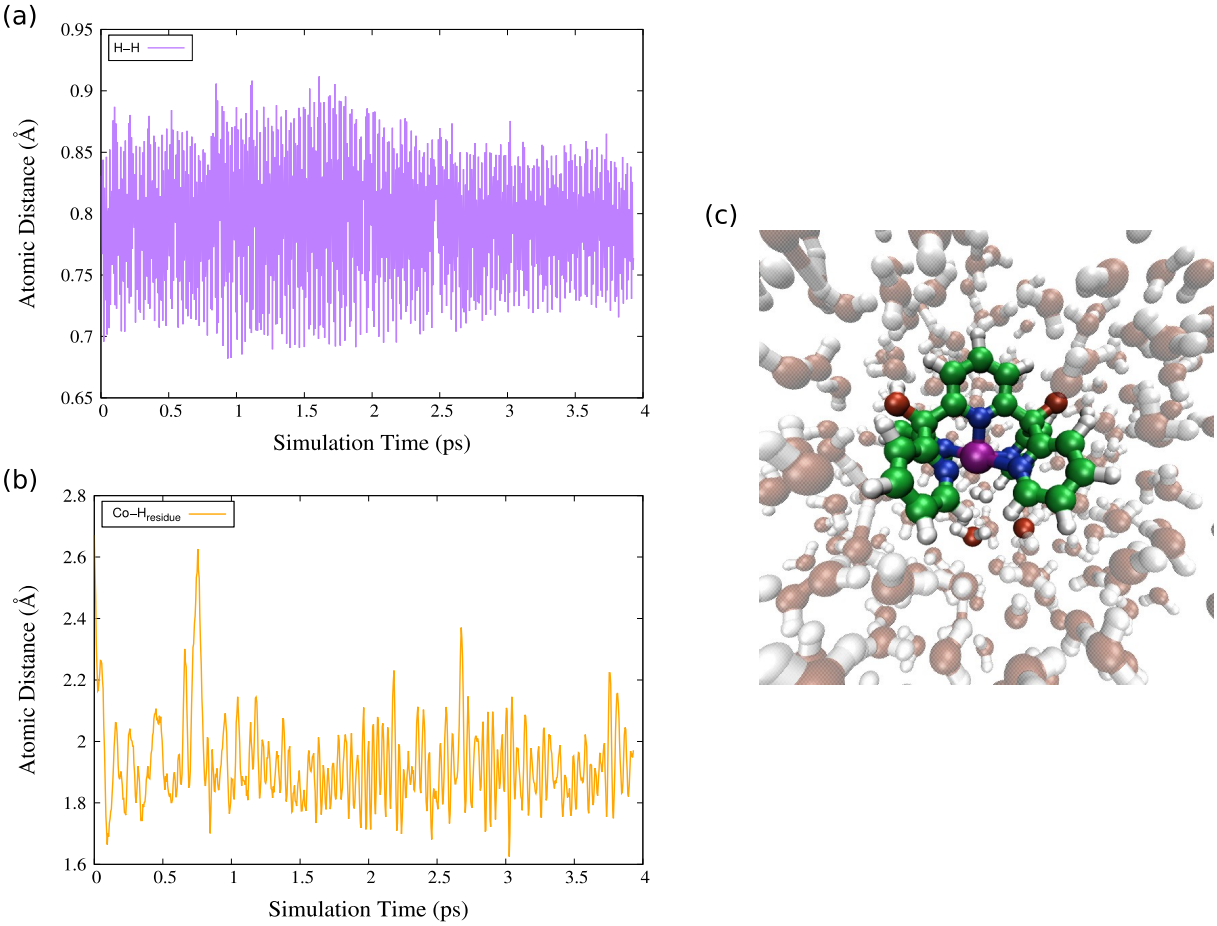

Figure 18: (a) H and H distances of the closest and different water molecules along the AIMD for the ECEC mechanism, $^{4}(CoPy_5)^{+2}$, are given. H-H distance is plotted in purple. (b) Co and H_2, Co-$H_{residue}$, distance along the the AIMD for $^{4}(CoPy_5)^{+2}$ is depicted in orange. (c) A snapshot is illustrated from the AIMD-NVT simulation $^{4}(CoPy_5)^{+2}$ trajectory at 4 ps of simulation time.

4.2 Intermediate Steps of the EECC Reaction Mechanism

We continue presentation of our results for the EECC reaction mechanism. At the EECC mechanism for H_2 production, two electron injection steps and two protonation steps in sequence are employed, see Figure 10-(b). The first step is the reduction reaction which is already modeled in the ECEC mechanism and we conclude that the reaction will proceed with the singlet spin state. Thus, we directly start modeling EECC reaction mechanism from the second reduction intermediate step using the initial configuration obtained by the singlet spin state trajectory.

Along with second electron injection, the spin state of the $CoPy_5$ becomes doublet with 0 total charge, $^2(CoPy_5)^0$. The AIMD-NVT snapshots are provided from 2 ps and 15 ps of the simulation are given in Figure 19-(a) and 19-(b), respectively. At the beginning of the simulation, the proton of the closest water molecule is attracted by the more negative Co center and remaining OH^- diffuses rapidly through the solvent. Co-H_{wat1} distance fluctuates around 2.2 Å at the beginning of the simulation, then at 2 ps of the simulation, H_{wat1} provides a coordination with the Co center and the distance between Co-H_{wat1} decreases to around 1.5 Å. Thus, the proton required for the first intermediate step of the reaction will be provided by this water molecule, see Figure 19-(c). The bond between Co-O_{wat1} fluctuates around 3 Å at the beginning of the simulation, afterwards, due to the fact that Co center binds to the proton of the water molecule and OH^- rapidly diffuses in solvent rapidly, this distance increases to 5 Å, see Figure 19-(d). The fact that hydroxyl anion rapidly diffuses in solvent by means of hydrogen bonds draws an inference that this step is not the rate limiting step for the reaction. In the contrary case, the hydroxyl anion which freely moves around the Co center likely retrieves the proton.

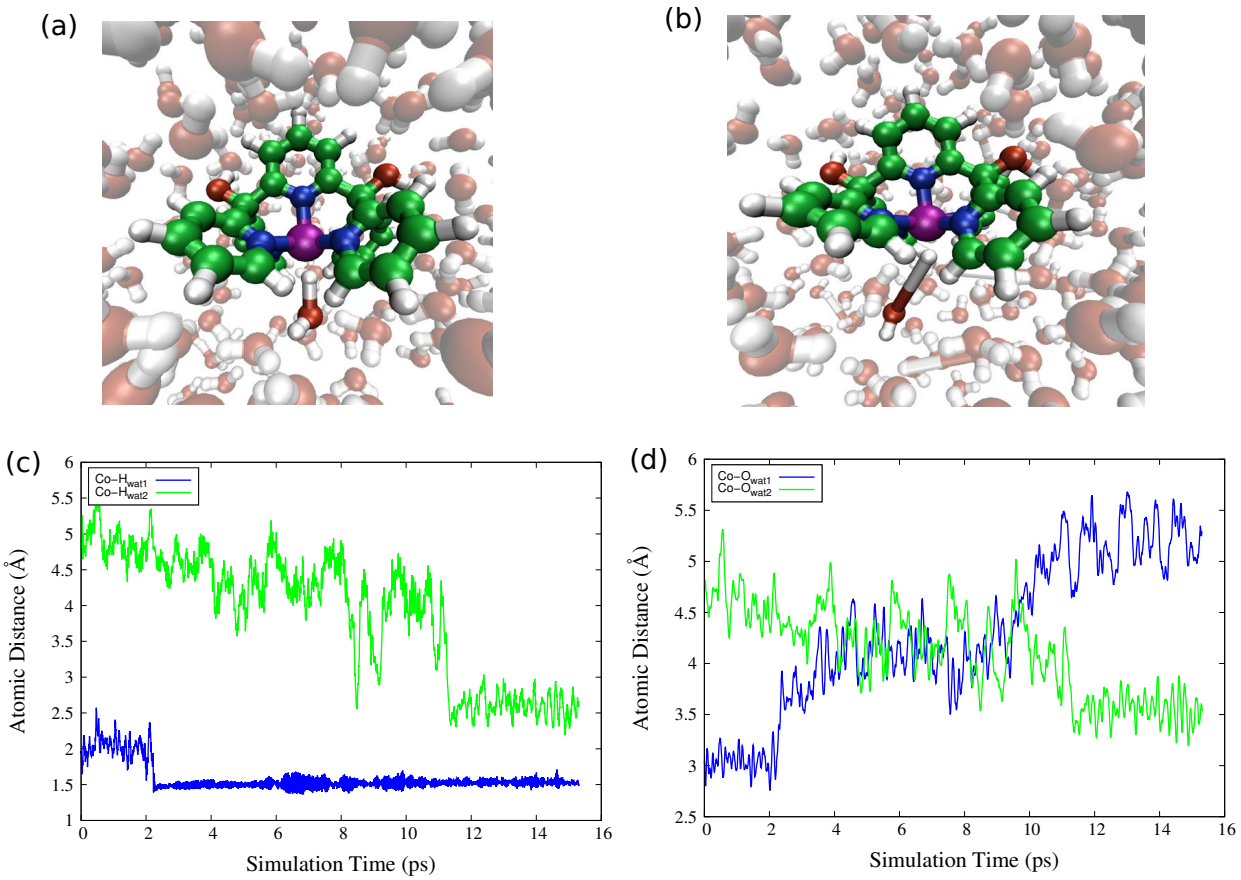

Figure 19: The second intermediate step of the EECC mechanism is depicted. The spin state of $CoPy_5$ is doublet and owns a total charge of 0, $^2(CoPy_5)^0$ a) A snapshot provided from AIMD simulation for doublet spin state of $CoPy_5$ in beginning of the simulation, 2 ps b) A snapshot provided from AIMD simulation for doublet spin state of $CoPy_5$ at end of the simulation, 15 ps c) The changes in distances between Co-H_{wat1} and Co-H_{wat2} with respect to the simulation time d) The fluctuations of the distances between Co-O_{wat1} and Co-O_{wat2} along the simulation.

The third step of the EECC mechanism is the first protonation. In order to put into practice the protonation step, a proton is added to the simulation box, far away from the catalyst and charge of the system remains unchanged. By this step, mechanism can have either doublet spin state or quartet spin state. In order to make a decision between doublet and quartet spin states, the distances between the closest water molecules and Co center should be examined for both cases by running simultaneous simulations having different spin states. Figure 20-(a) shows the distances between Co-H^+ and H_{wat1} and Co-H^+ and H_{wat2} which are plotted along the simulation time for the doublet spin state, $^2(CoPy_5)^{+1}$. Co-H^+ and H_{wat1} average distance is measured as around 2.6 Å along the simulation. On the other side, distance between Co-H^+ and H_{wat2} fluctuates around 4 Å at the beginning of the simulation and then increases to 4.5 Å

as simulation evolves. The AIMD-NVT snapshot provided from the simulation of the first protonation with doublet spin state is given at Figure 20-(c). Figure 20-(b) shows the distances between the Co-H^+ and $H_{wat1,}$ and Co-H^+ and H_{wat2} for quartet spin state of the system and Figure 20-(d) provides an AIMD snapshot of quartet spin state of the first protonation. Co-H^+ and H_{wat1} distance first remains stable at around 2.8 Å until the half time of the simulation and then increases up to 4.5 Å then again decreases to around 2.8 Å and preserves its stability until the end of the simulation. At the same time, distance between Co-H^+ and H_{wat2} fluctuates around 2.7 Å and remains stable along with entire simulation. At the modeled system with doublet spin state, only one proton provides a coordination with Co-H^+. On the other hand, with quartet spin state protons of two closest water molecules provide coordination with the Co center. Having two water molecules willing to donate their protons to the Co center of the catalyst is substantial part of determination of the spin state for the next step. As a result, quartet model is found to be more appropriate choice to continue the simulation of the H_2 production reaction mechanism.

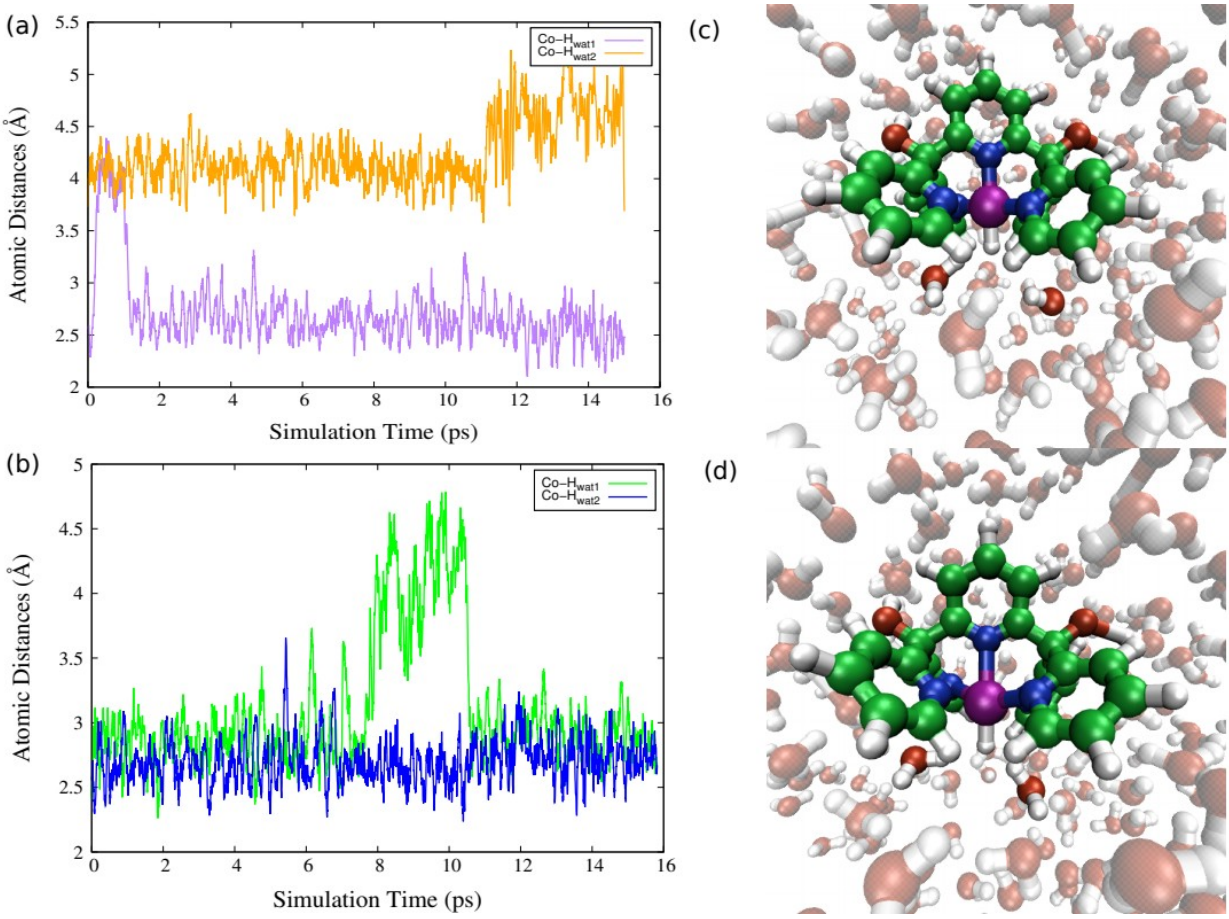

Figure 20: The third step of EECC mechanism are depicted. (a) Co-H_{wat1} and Co-H_{wat2} distances along the AIMD trajectory for $^{2}(CoPy_5)^{+1}$ which are depicted by purple and orange, respectively. (b) Co-H_{wat1} and Co-H_{wat2} distances along the AIMD for $^{4}(CoPy_5)^{+1}$ which are plotted by green and blue colors, respectively, where Co represents Co-H^{+} residue for both systems. (c) A snapshot is illustrated from the AIMD-NVT $^{2}(CoPy_5)^{+1}$ trajectory at 15 ps of simulation time. (d) A snapshot is illustrated from the AIMD-NVT $^{4}(CoPy_5)^{+1}$ trajectory at 16 ps of simulation time.

For the H_2 production step of the EECC mechanism, we expect formation of the H_2 following the second protonation, however the AIMD-NVT trajectory gives rather strange behavior observed for the H_2 formation. As it is depicted in Figure 21-(a), the distance between two hydrogens which should form H_2 increases from 1 Å to around 6 Å. This results denotes that, at the EECC mechanism of the H_2 production catalyzed by the $CoPy_5$ fails to form H_2 molecule. As it is depicted in Figure 21-(b), the distances between H-H residue and the Co center increases over the simulation time, which means, unlike the production step of the ECEC mechanism, at EECC mechanism the surrounding water molecules allow the protons to move freely resulting in Hs to move away from the Co center. The surrounding water molecules and their desire to receive the protons to form hydronium ions as well as the charge

density around the catalyst are considered as the reasons for failing H_2 bond formation, see Figure 21-(c). It is again interesting that the OH^- anion which provides the second proton does not diffuses to the solvent and does not interact with the protons in the close vicinity of the Co center. The OH^- anion is, instead, attracted to the proton which before formed a bond with the proton binded to Co center. This behavior will be analyzed further in detail by running additional simulations starting with different initial configurations.

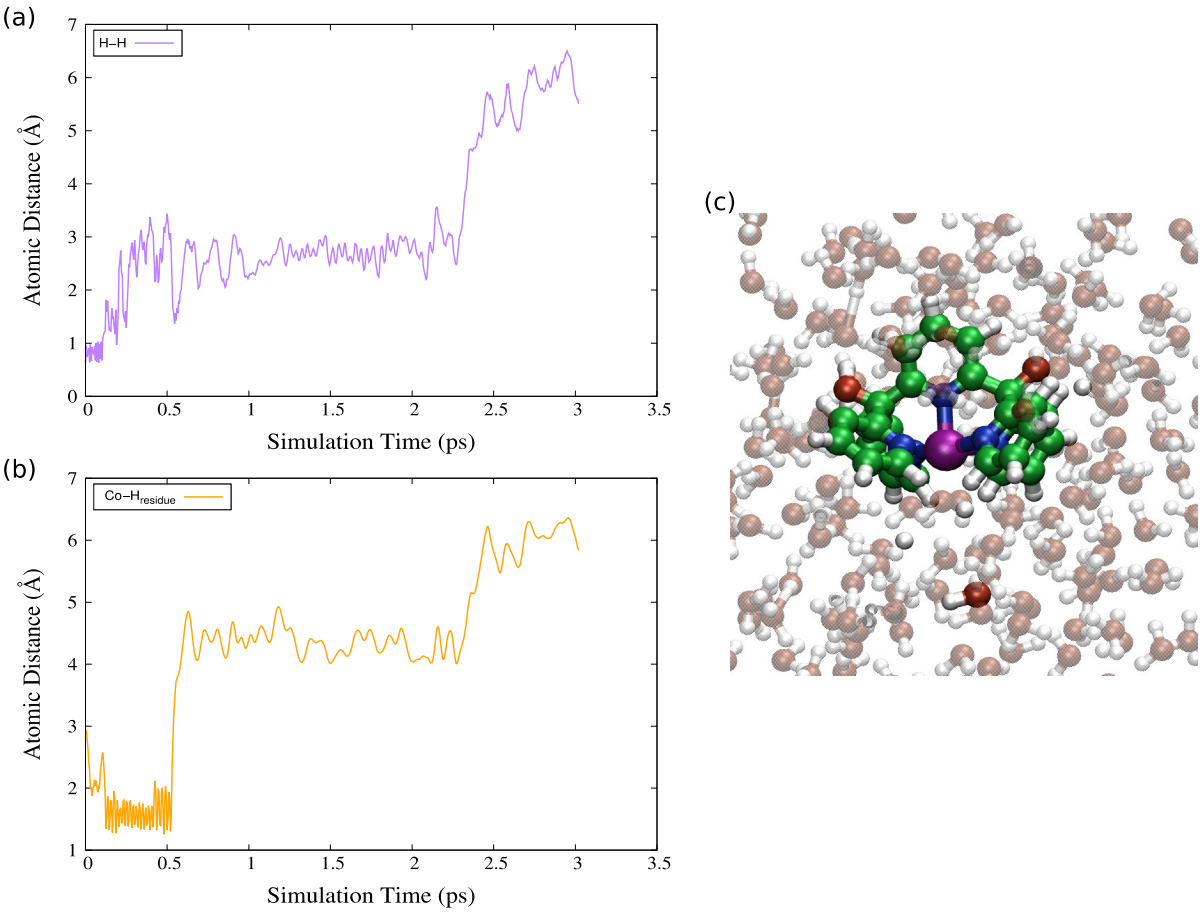

Figure 21: (a) H - H distance along the AIMD-NVT trajectory for the EECC mechanism for $^4(CoPy_5)^{+2}$ is plotted in purple. (b) Co and H, Co-$H_{residue}$, distance along the AIMD for $^4(CoPy_5)^{+2}$ is plotted in orange. (c) A snapshot illustrated from the AIMD-NVT $^4(CoPy_5)^{+2}$ trajectory at 3 ps of simulation time.

4.3 Structural Changes Observed For $CoPy_5$

Along the simulations of the H_2 production reaction, catalysts undergo some changes and accordingly these changes effect the distances between the pyridyl groups and the Co center. Alterations of mentioned distances has an important place to specify the geometry of catalyst. Table 1 and 2 shows the distances between pyridine rings, N_{RPy1}, N_{RPy2}, N_{LPy1}, N_{LPy2}, N_A and Co center for each step of the ECEC and EECC mechanisms, respectively. As it is shown in Table 1, distances between pyridine rings and Co center decreases after first reduction step, which is more effective for the singlet spin state. Depending on reducing the system, the catalyst band together and becomes a more compact system. First protonation has no significant effect on the bonds between Ns and Co. After second electron injection, a significant elongation of bonds between Ns and Co center are observed at both doublet and quartet spin multiplicities, however the effect is more visible at quartet spin state. Following the second protonation step of ECEC mechanism, namely H_2 production step, the production cycle come to the end and the charge and multiplicity of the catalyst return to the initial state.

Table 1: Distances between N of pyridyl groups and Co center of $CoPy_5$ immersed in water for each intermediate steps of the ECEC mechanism employed for H_2 production in water. 1st reduction is modeled using both triplet and singlet multiplicities. Second reduction is modeled for both doublet and quartet spin multiplicities. The distances are given in Å.

Step	***Formula***	$d_{N_{Rpy1}}$	$d_{N_{Rpy2}}$	$d_{N_{Lpy1}}$	$d_{N_{Lpy2}}$	d_{N_A}
Initial state	$^4(CoPy_5)^{+2}$	2.14	2.15	2.15	2.15	2.1
1st reduction	$^3(CoPy_5)^{+1}$	2.11	2.15	2.11	2.1	2.00
1st reduction	$^1(CoPy_5)^{+1}$	1.97	1.97	1.98	1.98	2.04
1st protonation	$^1(CoPy_5\text{-}H)^{+2}$	1.95	1.96	1.96	1.96	2.03
2nd reduction	$^2(CoPy_5\text{-}H)^{+1}$	2	2.13	2.19	2	1.97
2nd reduction	$^4(CoPy_5\text{-}H)^{+1}$	2.15	2.14	2.17	2.16	2.15
2nd protonation	$^4(CoPy_5)^{+2}\text{-}H_2$	2.15	2.1	2.14	2.14	2.03

Following the second reduction step of the EECC mechanism, more shrinkage of the bonds have been obtained with respect to the ECEC mechanism. Afterwards, any significant difference at bond lengths have been observed for the doublet spin multiplicity of the first protonation step. However, the bond elongation at quartet spin multiplicity for the same step has drawn attention. Lastly, the second protonation step gives rise to release of protons, accordingly, similarly to the ECEC mechanism, the bond lengths between Ns and Co center return back to the beginning with differences, see Table 2.

Table 2: Distances between N of pyridyl groups and Co center of $CoPy_5$ for intermediate steps on and after 2nd reduction of the EECC mechanism employed for H_2 production in water. 1st protonation step is modeled using both doublet and quartet spin multiplicities. The distances are given in Å.

Step	***Formula***	$d_{N_{Rpy1}}$	$d_{N_{Rpy2}}$	$d_{N_{Lpy1}}$	$d_{N_{Lpy2}}$	d_{N_A}
2nd reduction	$^2(CoPy_5)^0$	1.97	2.25	2.17	1.97	1.98
1st protonation	$^2(CoPy_5\text{-}H)^{+1}$	1.98	2.23	2.17	1.99	1.97
1st protonation	$^4(CoPy_5\text{-}H)^{+1}$	2.11	2.19	2.16	2.16	2.18
2nd protonation	$^4(CoPy_5)^{+2}\text{-}H_2$	2.13	2.11	2.12	2.12	2.11

4.4 Electronic Structure Analysis

It is evinced that the atomic rearrangements affects the interactions and behavior of the molecules as well as solvent response. Furthermore, these rearrangements of atomic structures also effect the electronic structures, consequently, in order to elucidate the electronic structure responses, we monitor the electronic structure evolution for each intermediate state of the reaction cycle. Here we consider only the initial state as well as pre and post spins of the reduction steps. The fluctuations of band gaps (eV) for the initial state, $^4(CoPy_5)^{+2}$, for the first reduced state, $^1(CoPy_5)^{+1}$, the first protonation at ECEC cycle, $^1(CoPy_5)^{+2}$, the second electron injection at the ECEC cycle, $^4(CoPy_5)^{+1}$ are depicted in Figure 22-(a). The band gap of initial state, $^4(CoPy_5)^{+2}$, fluctuates around 4 eV and at the first reduced state, $^1(CoPy_5)^{+1}$, band gap decreases and fluctuates around 2 eV. It is shown in Figure 22-(a), after first protonation,

$^{1}(CoPy_5)^{+2}$, catalyst's band gap shows wide fluctuations around 3.2 eV, increases from 2 eV and after the second electron injection, $^{4}(CoPy_5)^{+1}$, its band gap again decreases and shows wide fluctuations around 2 eV, which can be interpret as the catalyst oscillates between two states. In the meantime, the wide fluctuations can be correlated with unstable environment due to rapid hydrogen bond breakings and formations which are confirmatory for following protonation.

Band gap oscillations for the EECC mechanism obtained for the initial state, $^{4}(CoPy_5)^{2}$, the first electron injection, $^{1}(CoPy_5)^{1}$, and the second electron injection, $^{2}(CoPy_5)^{0}$, versus simulation time (ps) are given in Figure 22-(b). The initial state and first electron injection step are common states for both ECEC and EECC mechanisms, accordingly band gap values and interpretations of them are equal. For the second electron injection step of the EECC mechanism, $^{2}(CoPy_5)^{0}$, band gap increases from 2 eV and widely fluctuates around 2.9 eV, see Figure 22-(b).

The redistribution of molecular orbitals of the states are presented in Figure 22. For the initial state, $^{4}(CoPy_5)^{+2}$, HOMO and LUMO representations are obtained from 5 ps of the AIMD-NVT trajectory, see Figure 22-(c). HOMO is mainly located on the Co center and Ns, while LUMO is distributed mostly on N_{LPy1} and N_{LPy2}. Following the first electron injection, the distribution of HOMO starts from N_{APy} including Co center, proceeds at axial direction and ends at where the water molecule binds to Co. LUMO, on the other hand, is distributed mainly on bipyridine, N_{RPy1} and N_{RPy2}, see Figure 22-(d). For the first protonation of the ECEC mechanism, the HOMO is situated mainly on right bipyridine and is distributed over solvent molecules. Distributions of LUMO is on all over the Ns except N_{RPy2} and N_{LPy2} as well as some contributions are observed on the Co center, see Figure 22-(e). HOMO is distributed mainly on the Co-H^{+} residue for the second electron injection step of the ECEC mechanism, while LUMO is situated only on the Co center of the molecule, see Figure 22-(f). Figure 22-(g) shows the HOMO and LUMO distribution of the H_2 production step for the ECEC reaction mechanism. The HOMO distribution becomes dense around the Co center and parts of the N_{RPy1} and N_{LPy1} at horizontal direction. LUMO, on the other hand, is distributed above the Co center and all over the N_{APy} as well as N_{RPy1} and N_{LPy1}.

The distributions of HOMO for the second electron injection step of the EECC mechanism is intensified on the Co, coordinated H^{+} as well as on the pyridine rings. The corresponding LUMO is located on N_{APy} and posterior pyridine rings as well as part of the Co center and

frontier rings, see Figure 22-(h). For the first protonation step of the EECC mechanism, HOMO is mainly located on Co center, surrounding Ns and water molecules situated on both sides of the Co. At this step, LUMO distributions slide towards pyridine ring as shown in Figure 22-(i). Lastly, Figure 22-(j) shows the HOMO-LUMO distribution of H_2 production step for the EECC mechanism. HOMO for the H_2 production through EECC mechanism is distributed on the Co center and its vertical direction, whereas LUMO distribution is observed mainly on the Co center and parts of the N_{APy}, N_{RPy1} and N_{LPy1}.

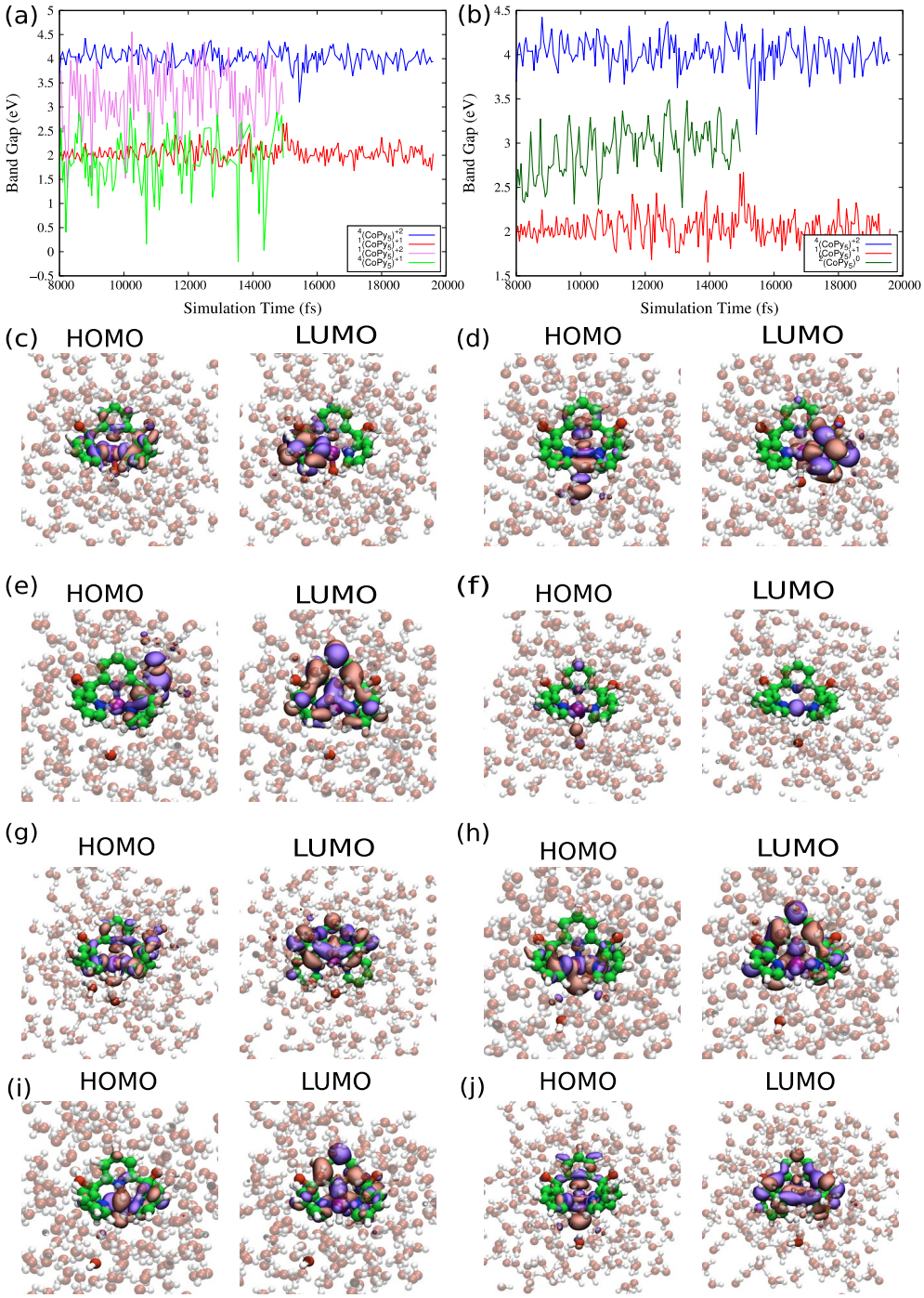

Figure 22: Along the AIMD simulations, the observed HOMO-LUMO gap for (a) the ECEC mechanism and (b) the EECC mechanism where blue: initial state $^{4}(CoPy_5)^{+2}$; red: the first electron injection, $^{1}(CoPy_5)^{+1}$; lilac: the first protonation $^{1}(CoPy_5)^{+2}$; green: the second electron injection $^{4}(CoPy_5)^{+1}$; dark green: the second electron injection $^{2}(CoPy_5)^{0}$ are given. The HOMO-LUMO distribution for (c) initial state $^{4}(CoPy_5)^{+2}$ at 4.5 ps, (d) reduced state $^{1}(CoPy_5)^{+1}$ at 13 ps, (e) first protonation for the ECEC mechanism $^{1}(CoPy_5\text{-}H)^{+2}$ at 6.4 ps, (f) the second electron injection for the ECEC mechanism $^{4}(CoPy_5)^{+1}$ at 8.8 ps, (g) the second protonation for the ECEC mechanism $^{4}(CoPy_5)^{+2}\text{-}H_2$ at 4 ps and, (h) the second electron injection for the EECC mechanism $^{2}(CoPy_5)^{0}$ at 13 ps, (i) the first protonation for the EECC mechanism $^{4}(CoPy_5\text{-}H)^{+1}$ at 11 ps. (j) the second protonation for the EECC mechanism $^{4}(CoPy_5)^{+2}\text{-}H_2$ at 3 ps. The isosurfaces are set to ±0.018 e/Å^3 positive depicted in pink and negative in purple.

4.5 Reduction Free Energies

In the course of this study, four electron injection steps have been performed. The first electron injection is the same step for both ECEC and EECC mechanisms, where $^{1}(CoPy_5)^{+1}$ or $^{3}(CoPy_5)^{+1}$ are the first reduced states and $^{4}(CoPy_5)^{+2}$ is the oxidized state. For the ECEC mechanism following the second electron injection, $^{4}(CoPy_5)^{+1}$ is the reduced state where $^{1}(CoPy_5)^{+2}$ is the oxidized state and finally, for the EECC mechanism $^{1}(CoPy_5)^{+1}$ and $^{2}(CoPy_5)^{0}$ are the oxidized and reduced states, respectively. In order to calculate the reduction free energies of the reduction steps, free energy perturbation theory has been employed. We use Marcus theory of electron transfer which assumes that electron transfer is very fast and during the electron injection nucleus does not change coordinates. This assumption also implies the linear solvent response to the electron transfer. Hence, by assuming the system with fixed coordinates, we add/remove electrons, form reduced and oxidized states and calculate the vertical energy differences between these states. We selected more than 180 snapshots from each of the AIMD-NVT trajectories modeling reduction reactions and applied hybrid density functional PBE0 together with rVV10 vdW density functional in order to increase accuracy of the calculated reduction free energies.

For the first electron injection, it is determined that it is more likely to continue with the singlet spin state due to the rapid solvent response and stability of the system. Therefore, for the first electron injection step, free energy calculations carried out only for the singlet spin state. The ensemble averages of the vertical energy differences $\langle \Delta E \rangle_R$ and $\langle \Delta E \rangle_O$ for the singlet spin state are estimated as -4.79 eV and 0.83 eV, respectively. Using Equation 1 given below, reduction free energy, ΔA_{E-O} , for singlet spin state of first electron injection calculated as, -1.98 eV.

$$\Delta A_{E-O} = \frac{1}{2}\left(\langle \Delta E \rangle_R + \langle \Delta E \rangle_O\right) \qquad (1)$$

The reorganization free energies are also calculated for each electron injection step in order to determine the energy needed for solvent molecules to reorganize themselves when any electronic effects occur at the system. As it is given at Table 3, reorganization energy of singlet spin state of the first electron injection is estimated as -2.81 eV with the employment

of Equation 2 given below. This large value can be explained by the water molecules situated around the catalyst rapidly change their positions due to the reduction of the catalyst.

$$\lambda = \frac{1}{2}\left(\langle \Delta E \rangle_R - \langle \Delta E \rangle_O\right) \tag{2}$$

The ensemble averages of the vertical energy differences of the reduced state for the second electron injection of the ECEC mechanism is estimated as -5.37 eV and for the oxidized state this difference is calculated as 1.04 eV. Reduction and reorganization free energies are obtained as -2.16 eV and -3.21 eV, respectively.

At the second electron injection of the EECC mechanism, $\langle \Delta E \rangle_R$ and $\langle \Delta E \rangle_O$ are calculated as -3.33 eV and 0.94 eV, respectively. Reduction free energy of this step is estimated as -1.20 eV and reorganization free energy is calculated as -2.13 eV, see Table 3. It can be concluded that the reorganization energy of the ECEC mechanism is higher than the EECC mechanism for the second electron transfer due to the breaking/formation of hydrogen bonds between water molecules situated around the catalyst for the ECEC mechanism.

Table 3: Reduction free energies (ΔA_{R-O}) and reorganization free energies (λ) for reduction reactions of the ECEC and EECC mechanisms are given in eV.

	First Electron Injection	Second Electron Injection ECEC	Second Electron Injection EECC
	Singlet Spin State	Quartet Spin State	Doublet Spin State
ΔA_{R-O}	-1.98	-2.16	-1.20
λ	-2.81	-3.21	-2.13

We analyze the energy differences between oxidized and reduced states and corresponding energy differences, ΔE , over the production time in picoseconds for the first reduction step as well as the second reduction steps of the ECEC and EECC mechanisms, see Figure 23-(a), (c) and (e), respectively. The frequencies of energy differences are depicted in Figure 23-(b), (d) and (f). The applicability of the reduction free energy formulations relay on the

fact that solvent shows linear behavior to the electron transfer implying that following the electron transfer we should not observe sudden solvent reorganization. This assumption can be verified by comparing the energy differences calculated for the oxidized and reduced limits. The width of the energy differences obtained for the reduced and oxidized limits should be similar to each other, so that linear solvent assumption holds and Marcus electron transfer theory could be used for calculating reduction free energies. From the Figure 23-(b), the widths for the vertical energy differences for the oxidized and reduced limits are similar to each other, thus calculated reduction free energy is, in principle, reliable. For the second electron injection step of the ECEC reaction mechanism, we observe significant differences in vertical energy gaps, see Figure 23-(d), which is attributed to the OH^- anion rapidly diffusing through the solvent. Thus, this step could show deviations from the linear solvent model.

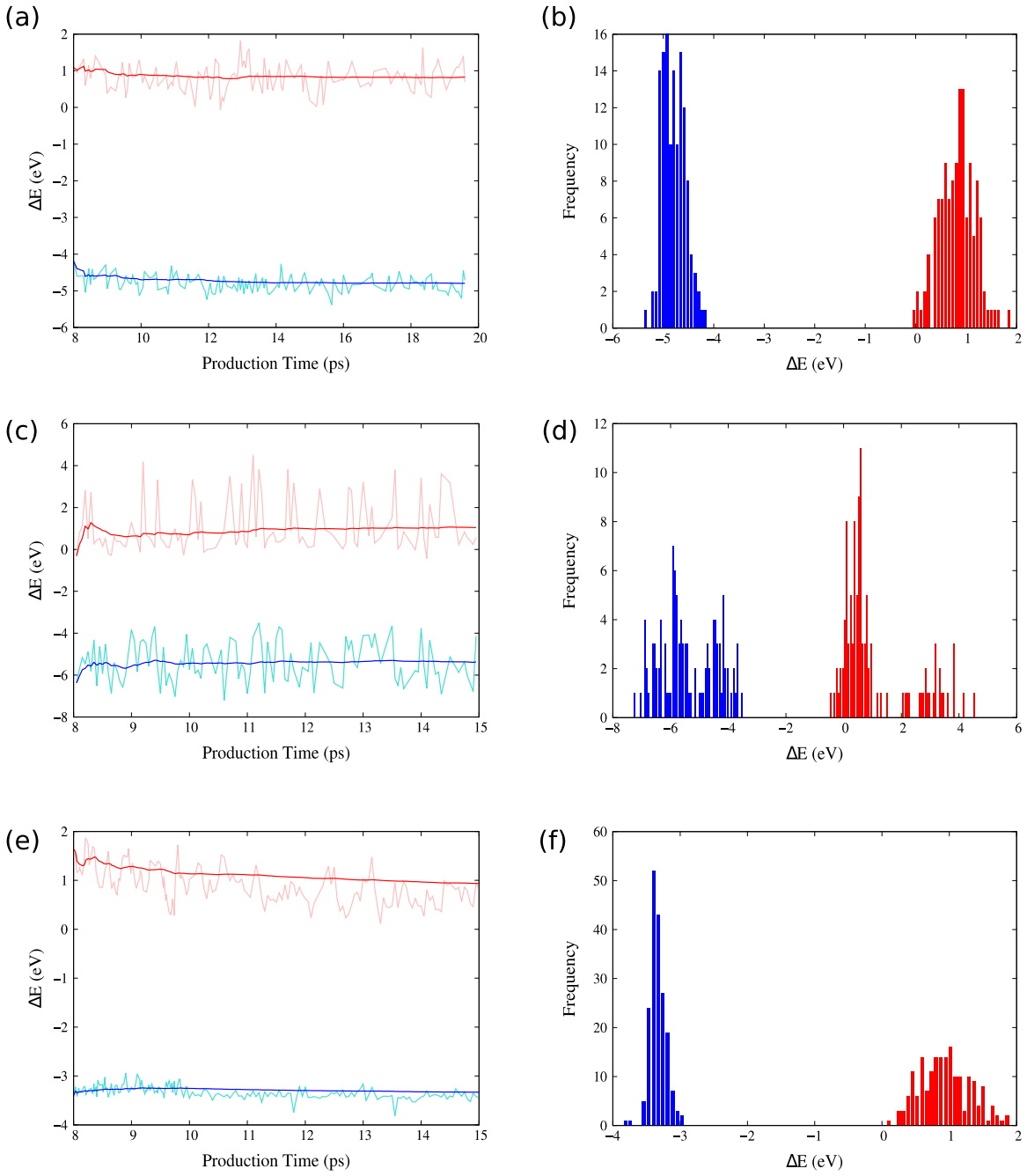

Figure 23: Line charts represents the energy differences and their accumulative averages of the first and second reduction reactions. Bar graphs show the frequencies of the energy differences. a) Energy differences versus production time (ps) of the first electron injection, $^{4}(CoPy_5)^{+2} + e^{-} \rightarrow {}^{1}(CoPy_5)^{+1}$, (b) Frequencies of the energy differences of the first reduction reaction, red for oxidation and blue for reduction. (c) Energy differences versus production time (ps) of the second electron injection of the ECEC mechanism, $^{1}(CoPy_5)^{+1} + e^{-} \rightarrow {}^{1}(CoPy_5)^{+2}$. (d) Frequencies versus energy differences for the second electron injection step of the ECEC mechanism (e) Energy differences versus production time (ps) of the second electron injection of the EECC mechanism, $^{1}(CoPy_5)^{+1} + e^{-} \rightarrow {}^{2}(CoPy_5)^{0}$. (f) Frequencies versus energy differences for the second electron injection step of the EECC mechanism. Turquoise lines represents the energy differences of the reduced limit and accumulative average shown with dark blue. Pink lines represents energy differences of oxidized limits and its accumulative averages shown with red.

5 CONCLUSIONS

In this thesis, we have elaborated the H_2 production mechanism of the $CoPy_5$ catalyst having penta-pyridyl ligand with perfect octahedral arrangement. We model the reaction mechanism using AIMD simulations in explicit water environment. We determine the spin states at each intermediate step and demonstrate the solvent response for each step. Following the first electron injection, one characteristics of the catalyst/water system to be noticed is that the water molecule coordinated with the Co changes its conformation shortly after the beginning of the simulation, allowing proton to generate a bond with the Co. Both triplet and singlet models demonstrate that the H_2 production reaction mechanism proceeds with singlet spin multiplicity. Subsequently, for the ECEC mechanism during the first protonation step, Co center gains the required proton from the water molecule in the first solvation shell. In an attempt to preserve the charge of the system, an extra proton has been embedded to the simulation box. Along the simulation, fast rotation of the nearest water molecule certifies the efficiency of the $CoPy_5$ for the water reduction reaction. An OH^- is formed neighbouring the Co center and supervenes establishing a hydrogen bond with the solvent. At the next step, mentioned as the second electron injection, the acquired results show that both doublet and quartet spin multiplicities are eligible for the reaction mechanism, however, resulting from pursuit of stability as well as the number of coordinated protons to the reaction center, we determine that the reaction is likely to continue with the quartet spin state. At the last step of ECEC mechanism which is the second protonation, our results show that the H_2 molecule have formed, however, it couldn't find a way to break away from the Co center which is unsuitable for the ideal situation. $CoPy_5$ molecule has a perfect octahedral arrangement and provides compact structure around the Co center, thus steric effects could, in principle, prohibit H_2 from diffusing towards the solvent and H_2 diffusion might be rate limiting step of the reaction.

Considering the EECC mechanism, following the first electron injection, the next step which is the second electron injection is simulated using doublet spin multiplicity with 0 charge. Subsequently, at the next step, the first protonation comes with two options to continue to the production cycle, which are doublet and quartet spin multiplicities and our results show that it is more likely to continue with quartet spin multiplicity. The reason is attributed to the fact that, compared to the doublet spin state, quartet spin state allows more than one proton

coordination with the Co center, thus Co would have more chance to be protonated for the next intermediate step. At the last step of the EECC mechanism which is the second protonation the system failed to form H_2 molecule. The reason of this situation is interpreted as Co center having “closed packed” environment tend to bond with the mentioned protons.

We have analyzed the electronic structures of the intermediate steps of both mechanisms in order to place the interpretations of our results on an electronic bases. Band gap fluctuations as well as HOMO and LUMO distributions of the catalyst/water systems have been determined.

Lastly, we have carried out free energy simulations for each step of both mechanisms in order to obtain reduction free energies and reorganization free energies of each electron injection steps. Our results show that the reduction free energy of the second electron injection step of the EECC mechanism has the least negative reduction free energy and the first electron injection step is less negative then the second electron injection step of the ECEC mechanism. The solvent reorganization energies of given states are slightly different from each other and again the ECEC mechanism shows the most negative value and the EECC mechanism is found to be the least negative one.

In conclusion, we aimed to extend the literature on the ECEC and EECC reaction mechanisms of the H_2 production by analyzing the catalytic response of the perfectly symmetric octahedral water reduction catalyst, $CoPy_5$. With this thesis, we provide a complete theoretical picture of the H_2 production mechanism of the $CoPy_5$ which will be useful for designing future water reduction catalysts.

REFERENCES

Alberto, R., Iannuzzi, M., Gurdal, Y., & Probst, B. (2019). [CoII(BPyPy2COH)(OH2)2]2+: A Catalytic Pourbaix Diagram and AIMD Simulations on Four Key Intermediates. *CHIMIA*, *73*(11), 906–906. https://doi.org/10.2533/chimia.2019.906

Ambrosio, F., Miceli, G., & Pasquarello, A. (2015). Redox levels in aqueous solution: Effect of van der Waals interactions and hybrid functionals. *The Journal of Chemical Physics*, *143*(24), 244508. https://doi.org/10.1063/1.4938189

Anantharaj, S., Ede, S. R., Karthick, K., Sankar, S. S., Sangeetha, K., Karthik, P. E., & Kundu, S. (2018). Precision and correctness in the evaluation of electrocatalytic water splitting: Revisiting activity parameters with a critical assessment. *Energy & Environmental Science*, *11*(4), 744–771. https://doi.org/10.1039/C7EE03457A

Anantharaj, S., Jayachandran, M., & Kundu, S. (2016). Unprotected and interconnected Ru0 nano-chain networks: Advantages of unprotected surfaces in catalysis and electrocatalysis. *Chemical Science*, *7*(5), 3188–3205. https://doi.org/10.1039/C5SC04714E

Bachmann, C., Guttentag, M., Spingler, B., & Alberto, R. (2013). 3d Element Complexes of Pentadentate Bipyridine-Pyridine-Based Ligand Scaffolds: Structures and Photocatalytic Activities. *Inorganic Chemistry*, *52*(10), 6055–6061. https://doi.org/10.1021/ic4004017

Barnett, R. N., & Landman, U. (1993). Born-Oppenheimer molecular-dynamics simulations of finite systems: Structure and dynamics of (${\mathrm{H}}_{2}$O${)}_{2}$. *Physical Review B*, *48*(4), 2081–2097. https://doi.org/10.1103/PhysRevB.48.2081

Basu, D., Mazumder, S., Niklas, J., Baydoun, H., Wanniarachchi, D., Shi, X., J. Staples, R., Poluektov, O., Bernhard Schlegel, H., & N. Verani, C. (2016). Evaluation of the coordination preferences and catalytic pathways of heteroaxial cobalt oximes towards hydrogen generation. *Chemical Science*, *7*(5), 3264–3278. https://doi.org/10.1039/C5SC04214C

Behnke, S. L., Manesis, A. C., & Shafaat, H. S. (2018). Spectroelectrochemical investigations of nickel cyclam indicate different reaction mechanisms for electrocatalytic CO2 and H+ reduction. *Dalton Transactions*, *47*(42), 15206–15216. https://doi.org/10.1039/C8DT02873G

Bhattacharjee, A., Andreiadis, E. S., Chavarot-Kerlidou, M., Fontecave, M., Field, M. J., & Artero, V. (2013). A Computational Study of the Mechanism of Hydrogen Evolution by Cobalt(Diimine-Dioxime) Catalysts. *Chemistry – A European Journal*, *19*(45), 15166–15174. https://doi.org/10.1002/chem.201301860

Bussi, G., Donadio, D., & Parrinello, M. (2007). Canonical sampling through velocity rescaling. *The Journal of Chemical Physics*, *126*(1), 014101. https://doi.org/10.1063/1.2408420

Cohen, A. J., Mori-Sánchez, P., & Yang, W. (2012). Challenges for Density Functional Theory. *Chemical Reviews*, *112*(1), 289–320. https://doi.org/10.1021/cr200107z

Dresselhaus, M., Crabtree, G., Buchanan, M., Mallouk, T., Mets, L., Taylor, K., Jena, P., DiSalvo, F., Zawodzinski, T., Kung, H., Anderson, I. S., Britt, P., Curtiss, L., Keller, J., Kumar, R., Kwok, W., Taylor, J., Allgood, J., Campbell, B., & Talamini, K. (2004). *Basic Research Needs for the Hydrogen Economy. Report of the Basic Energy Sciences Workshop on Hydrogen Production, Storage and Use, May 13-15, 2003*. DOESC (USDOE Office of Science (SC)); Argonne National Lab. (ANL), Argonne, IL (United States). https://doi.org/10.2172/899224

Ernzerhof, M., & Scuseria, G. E. (1999). Assessment of the Perdew–Burke–Ernzerhof exchange-correlation functional. *The Journal of Chemical Physics*, *110*(11), 5029–5036.

Esswein, A. J., & Nocera, D. G. (2007). Hydrogen Production by Molecular Photocatalysis. *Chemical Reviews*, *107*(10), 4022–4047. https://doi.org/10.1021/cr050193e

Goedecker, S., Teter, M., & Hutter, J. (1996). Separable dual-space Gaussian pseudopotentials. *Physical Review B*, *54*(3), 1703.

Grätzel, M. (2010). Photoelectrochemical cells. In *Materials for Sustainable Energy* (pp. 26–32). Co-Published with Macmillan Publishers Ltd, UK. https://doi.org/10.1142/9789814317665_0003

Grimme, S., Antony, J., Ehrlich, S., & Krieg, H. (2010). A consistent and accurate ab initio parametrization of density functional dispersion correction (DFT-D) for the 94 elements H-Pu. *The Journal of Chemical Physics*, *132*(15), 154104. https://doi.org/10.1063/1.3382344

Gritsenko, O. V., Schipper, P. R. T., & Baerends, E. J. (1997). Exchange and correlation energy in density functional theory: Comparison of accurate density functional theory quantities with traditional Hartree–Fock based ones and generalized gradient approximations for the molecules Li2, N2, F2. *The Journal of Chemical Physics*, *107*(13), 5007–5015. https://doi.org/10.1063/1.474864

Gürdal, Y. (2017). Theoretical Investigation of H_2 Generation Systems: From Homogenous to Heterogeneous Photo-Catalysis [Dissertation, University of Zurich]. In *Gürdal, Yeliz. Theoretical Investigation of H_2 Generation Systems: From Homogenous to Heterogeneous Photo-Catalysis. 2017, University of Zurich, Faculty of Science.* https://doi.org/10.5167/uzh-143485

Gurdal, Y., Hutter, J., & Iannuzzi, M. (2017). Insight into (Co) pyrphyrin adsorption on Au (111): Effects of herringbone reconstruction and dynamics of metalation. *The Journal of Physical Chemistry C*, *121*(21), 11416–11427.

Gurdal, Y., & Iannuzzi, M. (2017). DFT-based Theoretical simulations for photocatalytic applications using TiO2. *Titanium Dioxide*, 189.

Gurdal, Y., & Iannuzzi, M. (2020). Comparison of Penta and Tetra-pyridyl Cobalt-based Catalysts for Water Reduction: H $_2$ Production Cycle, Solvent Response and Reduction Free Energy. *ChemPhysChem*, cphc.202000600. https://doi.org/10.1002/cphc.202000600

Gurdal, Y., Luber, S., Hutter, J., & Iannuzzi, M. (2015). Non-innocent adsorption of Co-pyrphyrin on rutile(110). *Physical Chemistry Chemical Physics*, *17*(35), 22846–22854. https://doi.org/10.1039/C5CP02767E

Guttentag, M., Rodenberg, A., Bachmann, C., Senn, A., Hamm, P., & Alberto, R. (2013). A highly stable polypyridyl-based cobalt catalyst for homo- and heterogeneous photocatalytic water reduction. *Dalton Transactions (Cambridge, England: 2003)*, *42*(2), 334–337. https://doi.org/10.1039/c2dt31699d

Guttentag, M., Rodenberg, A., Kopelent, R., Probst, B., Buchwalder, C., Brandstätter, M., Hamm, P., & Alberto, R. (2012). Photocatalytic H_2 Production with a Rhenium/Cobalt System in Water under Acidic Conditions. *European Journal of Inorganic Chemistry*, *2012*(1), 59–64. https://doi.org/10.1002/ejic.201100883

Heyd, J., Scuseria, G. E., & Ernzerhof, M. (2003). Hybrid functionals based on a screened Coulomb potential. *The Journal of Chemical Physics*, *118*(18), 8207–8215. https://doi.org/10.1063/1.1564060

Hisatomi, T., Minegishi, T., & Domen, K. (2012). Kinetic Assessment and Numerical Modeling of Photocatalytic Water Splitting toward Efficient Solar Hydrogen Production. *Bulletin of the Chemical Society of Japan*, *85*(6), 647–655. https://doi.org/10.1246/bcsj.20120058

Hohenberg, P., & Kohn, W. (1964). Inhomogeneous Electron Gas. *Physical Review*, *136*(3B), B864–B871. https://doi.org/10.1103/PhysRev.136.B864

Huheey, J. E., Keiter, E. A., & Keiter, R. L. (n.d.). *Inorganic Chemistry: Principles of Structure and Reactivity (Harper Collins, New York, 1993).*

Islam, N., & Kaya, S. (2018). *Conceptual Density Functional Theory and Its Application in the Chemical Domain*. CRC Press.

Joliat, E., Schnidrig, S., Probst, B., Bachmann, C., Spingler, B., Baldridge, K. K., Rohr, F. von, Schilling, A., & Alberto, R. (2016). Cobalt complexes of tetradentate, bipyridine-based macrocycles: Their structures, properties and photocatalytic proton reduction. *Dalton Transactions*, *45*(4), 1737–1745. https://doi.org/10.1039/C5DT04426J

Joliat-Wick, E., Weder, N., Klose, D., Bachmann, C., Spingler, B., Probst, B., & Alberto, R. (2018). Light-Induced H_2 Evolution with a Macrocyclic Cobalt Diketo-Pyrphyrin as a Proton-Reducing Catalyst. *Inorganic Chemistry*, *57*(3), 1651–1655. https://doi.org/10.1021/acs.inorgchem.7b02992

Khnayzer, R. S., Thoi, V. S., Nippe, M., King, A. E., Jurss, J. W., Roz, K. A. E., Long, J. R., Chang, C. J., & Castellano, F. N. (2014). Towards a comprehensive understanding of visible-light photogeneration of hydrogen from water using cobalt(II) polypyridyl catalysts. *Energy & Environmental Science*, *7*(4), 1477–1488. https://doi.org/10.1039/C3EE43982H

Kohn, W., & Sham, L. J. (1965). Self-consistent equations including exchange and correlation effects. *Physical Review*, *140*(4A), A1133.

Kong, D., Zheng, Y., Kobielusz, M., Wang, Y., Bai, Z., Macyk, W., Wang, X., & Tang, J. (2018). Recent advances in visible light-driven water oxidation and reduction in suspension systems. *Materials Today*, *21*(8), 897–924. https://doi.org/10.1016/j.mattod.2018.04.009

Krukau, A. V., Vydrov, O. A., Izmaylov, A. F., & Scuseria, G. E. (2006). Influence of the exchange screening parameter on the performance of screened hybrid functionals. *The Journal of Chemical Physics*, *125*(22), 224106. https://doi.org/10.1063/1.2404663

Kühne, T. D., Iannuzzi, M., Del Ben, M., Rybkin, V. V., Seewald, P., Stein, F., Laino, T., Khaliullin, R. Z., Schütt, O., Schiffmann, F., Golze, D., Wilhelm, J., Chulkov, S., Bani-Hashemian, M. H., Weber, V., Borštnik, U., Taillefumier, M., Jakobovits, A. S., Lazzaro, A., … Hutter, J. (2020). CP2K: An electronic structure and molecular dynamics software package - Quickstep: Efficient and accurate electronic structure calculations. *The Journal of Chemical Physics*, *152*(19), 194103. https://doi.org/10.1063/5.0007045

Lee, C. H., Dogutan, D. K., & Nocera, D. G. (2011). Hydrogen Generation by Hangman Metalloporphyrins. *Journal of the American Chemical Society*, *133*(23), 8775–8777. https://doi.org/10.1021/ja202136y

Lee, C., Yang, W., & Parr, R. G. (1988). Development of the Colle-Salvetti correlation-energy formula into a functional of the electron density. *Physical Review B*, *37*(2), 785–789. https://doi.org/10.1103/PhysRevB.37.785

Leung, C.-F., Ng, S.-M., Ko, C.-C., Man, W.-L., Wu, J., Chen, L., & Lau, T.-C. (2012). A cobalt(II) quaterpyridine complex as a visible light-driven catalyst for both water oxidation and reduction. *Energy & Environmental Science*, *5*(7), 7903–7907. https://doi.org/10.1039/C2EE21840B

Lewis, N. S., & Nocera, D. G. (2006). Powering the planet: Chemical challenges in solar energy utilization. *Proceedings of the National Academy of Sciences*, *103*(43), 15729–15735. https://doi.org/10.1073/pnas.0603395103

Lucarini, F., Bongni, D., Schiel, P., Bevini, G., Benazzi, E., Solari, E., Fadaei-Tirani, F., Scopelliti, R., Marazzi, M., Natali, M., Pastore, M., & Ruggi, A. (2021). Rationalizing Photo-Triggered Hydrogen Evolution Using Polypyridine Cobalt Complexes: Substituent Effects on Hexadentate Chelating Ligands. *ChemSusChem*, *14*(8), 1874–1885. https://doi.org/10.1002/cssc.202100161

Marx, D., & Hutter, J. (2019). *Ab Initio Molecular Dynamics: Basic Theory and Advanced Methods*. Cambridge University Press.

Morin, J., & Pelletier, J. M. (2013). *Density functional theory: Principles, applications and analysis*. Nova Science Publishers, Incorporated.

Naimi, Y., & Antar, A. (2018). *Hydrogen Generation by Water Electrolysis*. 18.

Orio, M., Pantazis, D. A., & Neese, F. (2009). Density functional theory. *Photosynthesis Research*, *102*(2), 443–453. https://doi.org/10.1007/s11120-009-9404-8

Pal, S. (2018). Pyridine: A useful ligand in transition metal complexes. *Pyridine*, *57*.

Perdew, J. P., Burke, K., & Ernzerhof, M. (1996). Generalized gradient approximation made simple. *Physical Review Letters*, *77*(18), 3865.

Probst, B., Guttentag, M., Rodenberg, A., Hamm, P., & Alberto, R. (2011). Photocatalytic H_2 Production from Water with Rhenium and Cobalt Complexes. *Inorganic Chemistry*, *50*(8), 3404–3412. https://doi.org/10.1021/ic102317u

Probst, B., Rodenberg, A., Guttentag, M., Hamm, P., & Alberto, R. (2010). A Highly Stable Rhenium−Cobalt System for Photocatalytic H_2 Production: Unraveling the Performance-Limiting Steps. *Inorganic Chemistry*, *49*(14), 6453–6460. https://doi.org/10.1021/ic100036v

Queyriaux, N., Giannoudis, E., D. Windle, C., Roy, S., Pécaut, J., G. Coutsolelos, A., Artero, V., & Chavarot-Kerlidou, M. (2018). A noble metal-free photocatalytic system based on a novel cobalt tetrapyridyl catalyst for hydrogen production in fully aqueous medium. *Sustainable Energy & Fuels*, *2*(3), 553–557. https://doi.org/10.1039/C7SE00428A

Queyriaux, N., Jane, R. T., Massin, J., Artero, V., & Chavarot-Kerlidou, M. (2015). Recent developments in hydrogen evolving molecular cobalt(II)–polypyridyl catalysts. *Coordination Chemistry Reviews*, *304–305*, 3–19. https://doi.org/10.1016/j.ccr.2015.03.014

Rodenberg, A., Orazietti, M., Probst, B., Bachmann, C., Alberto, R., Baldridge, K. K., & Hamm, P. (2015). Mechanism of Photocatalytic Hydrogen Generation by a Polypyridyl-Based Cobalt Catalyst in Aqueous Solution. *Inorganic Chemistry*, *54*(2), 646–657. https://doi.org/10.1021/ic502591a

Rossmeisl, J., Dimitrievski, K., Siegbahn, P., & Nørskov, J. K. (2007). Comparing Electrochemical and Biological Water Splitting. *The Journal of Physical Chemistry C*, *111*(51), 18821–18823. https://doi.org/10.1021/jp077210j

Sabatini, R., Gorni, T., & de Gironcoli, S. (2013). Nonlocal van der Waals density functional made simple and efficient. *Physical Review B*, *87*(4), 041108. https://doi.org/10.1103/PhysRevB.87.041108

Schnidrig, S., Bachmann, C., Müller, P., Weder, N., Spingler, B., Joliat-Wick, E., Mosberger, M., Windisch, J., Alberto, R., & Probst, B. (2017). Structure–Activity and Stability Relationships for Cobalt Polypyridyl-Based Hydrogen-Evolving Catalysts in Water. *ChemSusChem*, *10*(22), 4570–4580. https://doi.org/10.1002/cssc.201701511

Skorodumova, N. V., Ahuja, R., Simak, S. I., Abrikosov, I. A., Johansson, B., & Lundqvist, B. I. (2001). Electronic, bonding, and optical properties of CeO 2 and Ce 2 O 3 from first principles. *Physical Review B*, *64*(11), 115108. https://doi.org/10.1103/PhysRevB.64.115108

Smolentsev, G., Soldatov, M. A., Probst, B., Bachmann, C., Azzaroli, N., Alberto, R., Nachtegaal, M., & van Bokhoven, J. A. (2018). Structure of the CoI Intermediate of a Cobalt Pentapyridyl Catalyst for Hydrogen Evolution Revealed by Time-Resolved X-ray Spectroscopy. *ChemSusChem*, *11*(18), 3087–3091. https://doi.org/10.1002/cssc.201801140

Song, X.-W., Meng, Y., Zhang, C.-L., Ma, C.-B., & Chen, C.-N. (2017). A cobalt complex of a pentadentate aminopyridine ligand as an efficient catalyst for photocatalytic hydrogen generation. *Inorganic Chemistry Communications*, *76*, 52–54. https://doi.org/10.1016/j.inoche.2017.01.011

Sun, Y., Bigi, J. P., Piro, N. A., Tang, M. L., Long, J. R., & Chang, C. J. (2011). Molecular Cobalt Pentapyridine Catalysts for Generating Hydrogen from Water. *Journal of the American Chemical Society*, *133*(24), 9212–9215. https://doi.org/10.1021/ja202743r

Teets, T. S., & Nocera, D. G. (2011). Photocatalytic hydrogen production. *Chemical Communications*, *47*(33), 9268–9274. https://doi.org/10.1039/C1CC12390D

Tong, L., Zong, R., & Thummel, R. P. (2014). Visible Light-Driven Hydrogen Evolution from Water Catalyzed by A Molecular Cobalt Complex. *Journal of the American Chemical Society*, *136*(13), 4881–4884. https://doi.org/10.1021/ja501257d

VandeVondele, J., & Hutter, J. (2007). Gaussian basis sets for accurate calculations on molecular systems in gas and condensed phases. *The Journal of Chemical Physics*, *127*(11), 114105. https://doi.org/10.1063/1.2770708

Varma, S., Castillo, C. E., Stoll, T., Fortage, J., Blackman, A. G., Molton, F., Deronzier, A., & Collomb, M.-N. (2013). Efficient photocatalytic hydrogen production in water using a cobalt(III) tetraaza-macrocyclic catalyst: Electrochemical generation of the low-valent Co(I) species and its reactivity toward proton reduction. *Physical*

Chemistry Chemical Physics, *15*(40), 17544–17552. https://doi.org/10.1039/C3CP52641K

Vydrov, O. A., & Van Voorhis, T. (2009). Nonlocal van der Waals Density Functional Made Simple. *Physical Review Letters*, *103*(6), 063004. https://doi.org/10.1103/PhysRevLett.103.063004

Wang, M., Na, Y., Gorlov, M., & Sun, L. (2009). Light-driven hydrogen production catalysed by transition metal complexes in homogeneous systems. *Dalton Transactions*, *33*, 6458–6467. https://doi.org/10.1039/B903809D

Wang, Y., Suzuki, H., Xie, J., Tomita, O., Martin, D. J., Higashi, M., Kong, D., Abe, R., & Tang, J. (2018). Mimicking Natural Photosynthesis: Solar to Renewable H_2 Fuel Synthesis by Z-Scheme Water Splitting Systems. *Chemical Reviews*, *118*(10), 5201–5241. https://doi.org/10.1021/acs.chemrev.7b00286

Watts, N., Amann, M., Arnell, N., Ayeb-Karlsson, S., Beagley, J., Belesova, K., Boykoff, M., Byass, P., Cai, W., Campbell-Lendrum, D., Capstick, S., Chambers, J., Coleman, S., Dalin, C., Daly, M., Dasandi, N., Dasgupta, S., Davies, M., Di Napoli, C., … Costello, A. (2021). The 2020 report of The Lancet Countdown on health and climate change: Responding to converging crises. *The Lancet*, *397*(10269), 129–170. https://doi.org/10.1016/S0140-6736(20)32290-X

Xie, J., Zhou, Q., Li, C., Wang, W., Hou, Y., Zhang, B., & Wang, X. (2014). An unexpected role of the monodentate ligand in photocatalytic hydrogen production of the pentadentate ligand-based cobalt complexes. *Chemical Communications*, *50*(49), 6520–6522. https://doi.org/10.1039/C4CC01471E